AMERICAN UNIVERSITY OF BEIRUT

GRAPHENE-BASED POLYMER COMPOSITE MATERIALS

by
ALI AMIN TARHINI

A dissertation
submitted in partial fulfillment of the requirements
for the degree of Doctor of Philosophy
to the Department of Mechanical Engineering
of the Maroun Semaan Faculty of Engineering and Architecture
at the American University of Beirut

Beirut, Lebanon
January 2022

AMERICAN UNIVERSITY OF BEIRUT

GRAPHENE-BASED POLYMER COMPOSITE MATERIALS

by

ALI AMIN TARHINI

Approved by:

Dr Ali Tehrani, Associate Professor
Baha and Walid Bassatne Department of Chemical Engineering and Advanced Energy, AUB
Ali Tehrani
Advisor

Dr Kamel Abougali, Professor
Department of Mechanical Engineering, AUB
Kamel Aboughali
Chair of Committee

Dr Michel Kazan, Associate Professor
Department of Physics, AUB
Member of Committee

Dr Samir Mustapha, Associate Professor
Department of Mechanical Engineering, AUB
Samir mustapha
Member of Committee

Dr Gilles Lubineau, Professor
Associate Dean Faculty, Physical Science and Engineering, KAUST
gilles lubineau
Member of Committee

Dr Ahmed Abdala, Professor
Department of Chemical Engineering, Texas A&M
Member of Committee

Date of dissertation defense: January 13, 2022

AMERICAN UNIVERSITY OF BEIRUT

DISSERTATION RELEASE FORM

Student Name: ___TARHINI_____ALI_____AMIN_____
Last First Middle

I authorize the American University of Beirut, to: (a) reproduce hard or electronic copies of my project; (b) include such copies in the archives and digital repositories of the University; and (c) make freely available such copies to third parties for research or educational purposes:

☒ As of the date of submission

☐ One year from the date of submission of my project.

☐ Two years from the date of submission of my project.

☐ Three years from the date of submission of my project.

_____ _____January 24, 2022_____

Signature Date

ACKNOWLEDGEMENTS

First and foremost, I am extremely grateful to my supervisor, Prof. Ali Tehrani for his invaluable advice, continuous support, and patience during my PhD study. His immense knowledge and plentiful experience have encouraged me in all the time of my academic research and daily life. I would like also to thank all the members in my committee. It is their kind help and support that have made me write this dissertation. Finally, I would like to express my gratitude to my parents, my wife and my lovely newborn child Mahdi. Without their tremendous understanding and encouragement in the past few years, it would be impossible for me to complete my study.

ABSTRACT

OF THE DISSERTATION OF

Ali Amin Tarhini for Doctor of Philosophy
Major: Mechanical Engineering

Title: Graphene-based Polymer Composite Materials

Polymer composites with enhanced physical and mechanical properties are of great interest in many applications (e.g., E-textile, wearable electronics, heat sinks, sensors, batteries). Such light, durable, and cheap material can partially replace metals and ceramics to save energy and cost. Adding graphene in a polymer matrix has been employed to achieve such an enhancement.

However, the obtained properties of these composites were generally much lower than expected. The challenge is that many parameters like the orientation of graphene layers, the type of graphene used, and the preparation method play an essential role in dictating the properties of the composites obtained. The goal of this study is to develop a smooth, scalable, and robust method to make highly aligned graphene-based polymer composite films with enhanced mechanical properties and ultra-high thermal and electrical conductivity values that can be used in many applications. Also, in this work the effect of various parameters (e.g. the type of graphene used, the lateral size of graphene flakes and filler weight content %) were analyzed. Several characterization techniques like (Scanning Electron Microscopy, X-Ray Diffraction, Differential Scanning Calorimeter, Raman Optothermal Spectroscopy, and Laser Flash Diffusivity Analyzer) were used to study these composites. The effect of temperature was also studied on the mechanical, thermal, and electrical properties of obtained composites. For the best of our knowledge, our results showed a high new record for in-plane thermal conductivity and electrical conductivity values of graphene-based polymer composite films, which demonstrate the importance and novelty of this research.

TABLE OF CONTENTS

ACKNOWLEDGEMENTS 1

ABSTRACT 2

ILLUSTRATIONS 6

TABLES 9

INTRODUCTION 10

GRAPHENE, POLYMERS, AND POLYMER COMPOSITES 10

A. POLYMERS 10

B. POLYMER COMPOSITES 11

C. GRAPHENE PROPERTIES 13

D. MATERIAL PROPERTIES 14

1. Thermal Properties 14

2. Electrical Properties 17

3. Mechanical Properties 18

E. POSSIBLE APPLICATIONS 18

1. Electronic Devices 19

2. Energy Storage 19

3. E-textile 20

4. Thermal Interface Materials (TIM) 21

5. Biomedical Applications 22

REVIEW OF LITERATURE.....24

GOAL AND RESEARCH OBJECTIVES.....32

A. Studying the incorporation of Graphene flakes in polymers (PVDF-HFP and PEMMA) 32

B. Analyzing the Mechanical Properties of obtained composites 33

C. Studying the Electrical Properties of obtained composites.....33

D. Studying the thermal Properties of obtained composites.....34

METHODOLOGY 35

A. Fabrication of GNF/polymer composite films.....35

B. Instruments Used for Characterization.....38

1. Scanning Electron Microscopy (SEM) 38
2. ATR-FTIR 39
3. X-ray diffraction (XRD) 39
4. Optical Tensiometer.....40
5. Other Equipment.....41

RESULTS AND DISCUSSIONS 46

A. Solvent mixing of Graphene Flakes in PVDF-HFP polymer (Based on Paper 1) 46

1. Characterizations of graphene-based PVDF-HFP composites 46
2. Mechanical properties.....51
3. Thermal conductivity.....52

B. Testing Solvent Mixing process with another polymer (PEMAA) and Comparing results between laser flash and OTR methods (Based on Paper 2) 55

C. Studying the effect of Graphene average particle size on thermal, electrical, and mechanical properties of polymer composites obtained (Based on Paper 3) 67

D. Studying the effect of temperature on thermal, electrical, and mechanical properties of polymer composites obtained (Based on Paper 4) 74

SUMMARY AND CONCLUSIONS.....86

APPENDIX A.....88

REFERENCES 90

ILLUSTRATIONS

Figure

1. The global production of plastics and steel by volume for the last decades [1] . 10
2. Thermal conduction mechanism in a composite is a function of filler size and w.t % [5] 12
3. Recent advances in thermal conductive materials with different electrical properties [6] 13
4. Graphene and its descendants: (a) graphene (b) graphite (c) nanotube: rolled graphene (d) fullerene: wrapped graphene [18] 14
5. Selected Thermal Conductivity values for some materials [19] 15
6. Thermal conduction mechanism in crystalline structures and polymers [5] 16
7. Smart clothing that is electrically conductive embedding a Temperature sensor with a display screen on a winter jacket (Image Source: Thread in Motion) 21
8. (a) Schematic illustrating electronic devices with interface materials bridging the heater and the heat sink. (b) The functionality of thermal interface materials that help in dropping the temperature when filling out the gaps in electronic devices [31] 22
9. Biosensors and components on a graphene platform [33] 23
10. (a) Setup scheme for home-made Raman spectroscopy integrated with laser (λmax =532 nm) (b) Setup scheme for laser flash method to measure in-plane thermal conductivity 26
11. Graphene/PVDF composite preparation process and conductivity values as proposed by Jung et al. [22] 27
12. Conduction mechanisms in a composite with increasing filler content [25] 34
13. OCA15 Optical Tensiometer 41
14. SEM micrographs of the composite films obtained for different w.t.% of GNF (a) neat PVDF-HFP (b) 10 GNF w.t.% (c) 20 GNF w.t.% [Colored figure] 47
15. Cross-section scanning electron microscopy images of PVDF-HFP-GN20 at two different magnifications [colored figure]. 48
16. (a) ATR-FTIR analysis for Graphene composite films (b) TGA of GNF/PVDF-HFP composite films under N2 atmosphere 49
17. (a) Stress-strain curves of the composites (b) The enhancement of the tensile strength and Young's modulus as a function of GNF content in the composites (d and e) two photographs showing the flexibility of PVDF-HFP-GN20 52

18. Thermal conductivity and Thermal conductivity enhancement as a function of GNF w.t. % 53

19. A scheme showing the transport of electron and phonon across the tilted and aligned Graphene layers within the GNF/PVDF-HFP composites 55

20. Raman Spectrum of a Silicon wafer obtained with a sharp peak at ~520 cm^{-1}.. 59

21. Raman Spectrum of Graphene-based polymeric composite PVDF-HFP-GN33 under 5 mW laser power 60

22. Raman Spectrum of Graphene-based polymeric composite PVDF-HFP-GN33 under 4 mW laser power 61

23. G peak shift in the Raman Spectrum of Graphene-based polymeric composite PVDF-HFP-GN33 at different laser powers (25,5,4,3,2,1 mW) 62

24. The Raman Spectrum of PVDF-HFP composites (a) PVDF-HFP-GN10 (b) PVDF-HFP-GN20 at 5 mW and 3 mW laser power 63

25. The Raman Spectrum of PEMAA composites (a) PEMAA-GN10 (b) PEMAA-GN20 (c) PEMAA-GN33 using different laser powers (25,5,3,2 mW) 64

26. (a) In-plane thermal conductivity of graphene-based PVDF-HFP composites (b) In-plane thermal conductivity of graphene-based PEMAA composites 67

27. Statistical analysis of average flake size for the three different types of Graphene (G1, G2, and G3) as a function of the number of flakes taken into account. The average flake size converges to the asymptotic average values 68

28. (a) ATR-FTIR analysis for G1, G2, and G3 (b) X-ray diffraction patterns for G1, G3, and G3 (c) Raman signal for G1 (d) Raman signal for G2 (e) Raman signal for G3 (f) Table showing the elemental analysis done on G1, G2, and G3..... 69

29. In-plane electrical conductivity as a function of graphene content (wt.%) for three different graphene types (a,b), and a picture showing a light bulb under 9V battery where PVDF-HFP-G1-20 film was used as an electrical connection (c). SEM micrographs 71

30. The Raman signals of Graphene-based composites (d) G-peak wavenumber versus Temperature (e) Enhancement of in-plane thermal conductivity as a function of Graphene content for three Graphene types G1, G2, and G3 72

31. Mechanical properties as a function of Graphene content (wt %) for three different Graphene types (a) G1 (b) G2 (c) G3 (d) Two photos showing the flexibility of PVDF-HFP-G1-20. [colored figures] 73

32. DSC diagrams of composite films: (a) PC-Gn 1% (b) PC-Gn 10% (c) PC-Gn 20 % 76

33. Storage modulus, loss modulus and tan δ curves from dynamic mechanical analysis (DMA) for the following films (a) PVDF-HFP (b) PC-Gn 1% (c) PC-

Gn 5% (d) PC-Gn 10% (e) PC-Gn 20% (f) variation of storage modulus and loss modulus as a function of graphene 76

34. (a) Electrical conductivity (EC) as a function of graphene content (wt%) across a temperature range between 25 °C and 125 °C for PC-Gn 1%, PC-Gn 5%, PC-Gn 10%, and PC-Gn 20% composite films (b) EC for PC-Gn 20% as a function of temperature (c) EC at T 25 79

35. (a) CV, (b) CSC, (c) EIS for for PVDF-HFP, PC-Gn 1%, PC-Gn 5%, PC-Gn 10%, and PC-Gn 20% composite films 82

36. Thermal conductivity (TC) values for PC-Gn films as a function of temperature 83

TABLES

Table

1. Electrical and Thermal conductivity for different metallic and carbon fillers [2] 11
2. Properties of Graphene-based polymer composite materials 24
3. Recipes for the preparation of GNF/PVDF-HFP composites paper 1 37
4. Thermal stability and degradation data of the composite films from TGA under Nitrogen Atmosphere 50
5. In-plane thermal conductivity values obtained using laser flash and Raman technique for graphene-based composites: GNF/PVDF-HFP and GNF/PEMAA 66
6. Charge-storage capacity (CSC) for different materials used as electrodes 82

CHAPTER I

INTRODUCTION

GRAPHENE, POLYMERS, AND POLYMER COMPOSITES

A. POLYMERS

Polymers are robust, lightweight, and easy to work within many applications, especially in the packaging industry. They are composed of long molecular chains of repeated structural units like ethylene, propylene, and vinyl chloride. Their low cost and ease of manufacturing attracted many industries like aviation, construction, and automotive to use this material in their applications. This huge demand was clearly reflected in the global production of plastics where it surpassed Steel since 1989 as shown in Figure 1. However, most polymers have shallow thermal and electrical conductivity values and poor mechanical properties, which limit their use in many applications.

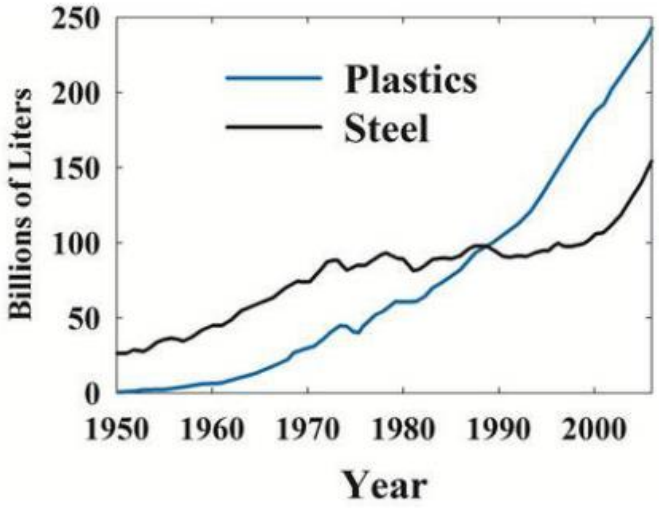

Figure 1 The global production of plastics and steel by volume for the last decades [1]

B. POLYMER COMPOSITES

Polymers can be reinforced by fillers to form composites with enhanced mechanical and physical properties. Fillers and additives can be added to tune the features of the polymer for specific application. There are two main kinds of conductive fillers: Carbon-based and metallic fillers. Carbon-based fillers include graphite, graphene, carbon nanotubes (CNT), carbon fibers, and carbon black. For metallic fillers, there are metallic powders, metal flakes, metal-coated fibers, and metal nanowires. Table 1 shows the electrical and thermal conductivity values of some metallic and carbon-based fillers.

Table 1 Electrical and Thermal conductivity for different metallic and carbon fillers [2]

Filler material	Electrical conductivity (S/cm)	Thermal Conductivity (W/mK)	Density (g/cm^3)
Aluminum	3.538×10^5	234	2.7
Copper	5.977×10^5	386-400	8.9
Silver	6.305×10^5	417-427	10.53
Nickle	1.43×10^5	88.5	8.9
CNTs	3.8×10^5	2000-6000	2.1
Carbon Fibers	10^2-10^5	10-1000	1.5-2.0
Graphene	6000	4000-7000	1.06

Graphite	10^4	100-500	2.25

Many factors affect the properties of obtained composites, such as the characteristics of the filler, the orientation of the filler in the polymer matrix, the loading of the filler, and the interface between the filler and the polymer matrix [3,4]. Figure 2 shows the mechanism of heat transfer in these composites, which is affected by the filler size, the compatibility between the filler and the matrix, the thermal conductivity of the filler, the presence of defects due to the preparation process, and the aspect ratio of the filler [5].

Different methods can be used to prepare a polymer composite with enhanced properties, including mixing and molding process, melt blending, in-situ polymerization, and layer by layer assembly [2]. The key for each of these preparation methods is the uniform distribution of the filler into the polymer matrix. These fillers can form a conductive network providing a path for heat and electrons with low resistance and little scattering across the interface between the filler and the polymer matrix.

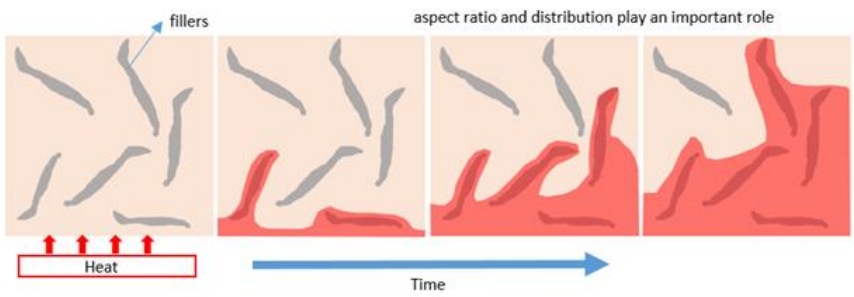

Figure 2 Thermal conduction mechanism in a composite is a function of filler size and w.t % [5]

Recent advances in thermally conductive materials with different electrical properties can be summarized in Figure 3. Polymer composites are classified as

semiconductors with relatively good thermal and electrical conductive properties. They did not reach the properties of metals yet. However, the low cost, lightweight, and resistance to corrosion are factors that make this material compete with metals in many applications, especially aerospace applications where weight is critical. Therefore, polymers with low thermal and electrical conductivities could be shifted to the upper right corner by adding Graphene-based filler, as shown in Figure 3 [6].

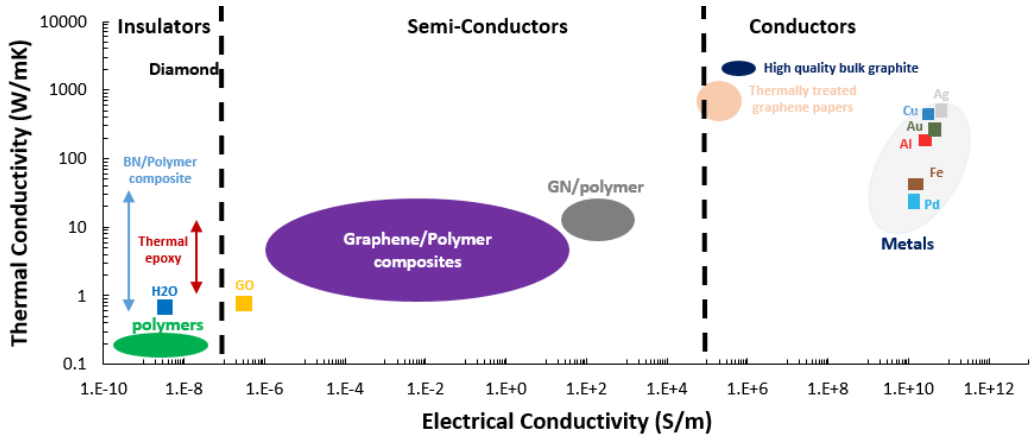

Figure 3 Recent advances in thermal conductive materials with different electrical properties [6]

C. GRAPHENE PROPERTIES

Graphene has some impressive properties, such as excellent mechanical properties, high electrical and thermal conductivity [7,8]. The research on Graphene and Graphene-based composites attracted tremendous academic and industrial interest after 2004 [9]. Graphene has a unique 2D structure, as shown in Figure 4 with the respective descendants: (1) Graphite (stack of Graphene layers) (2) Carbon nanotube (rolled graphene) (3) Fullerene (wrapped graphene). This unique 2D structure for Graphene ensures an exceptional in-plane thermal conductivity (κ) [10]. A suspended single-layer Graphene has in-plane thermal conductivity value (κ) around 3080–5150 W m^{-1} K^{-1} at

room temperature, which is the highest of any currently known materials [11,12]. Also, Graphene has impressive mechanical properties where Young's modulus and intrinsic strength of a free-standing Graphene monolayer can reach up to 1 TPa and 130 GPa, respectively. These values are nearly 100 times higher than the reported values for a steel sheet provided that they have an identical thickness [13,14]. These high mechanical and physical properties have attracted many researchers to use Graphene and its derivatives as fillers in polymer composites to dramatically enhance the properties of polymers, as shown in Figure 3 [15–17].

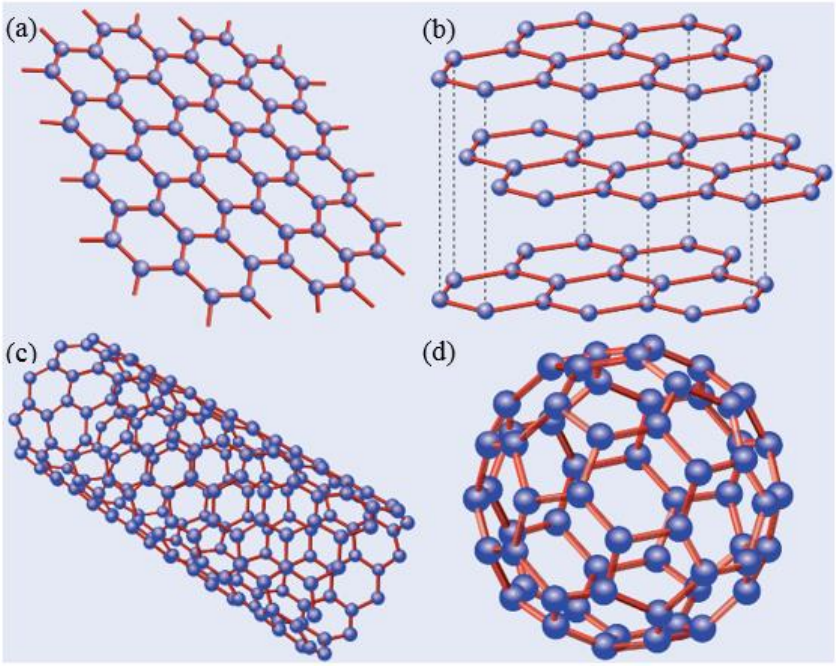

Figure 4 Graphene and its descendants: (a) graphene (b) graphite (c) nanotube: rolled graphene (d) fullerene: wrapped graphene [18]

D. MATERIAL PROPERTIES

1. Thermal Properties

Most polymers have very low thermal conductivities in the range of 0.1 - 0.5 W m^{-1} $K^{-1,}$ as shown in Figure 5. In contrast, metals have very high thermal conductivity that can reach up to 385 W m^{-1} K^{-1} for Copper, for example. The reason behind that is

that polymers are mainly made from chains of repeated structural units [e.g., ethylene, propylene, vinyl chloride, styrene]. In amorphous polymers, heat first reaches the first layer, which is schematically the closest to the heat source. The heat is then transferred to the adjacent atom sequentially without propagating as a wave, as in crystal structures like metals where heat diffuses with the standard vibrational mode at the same speed between all particles [5].

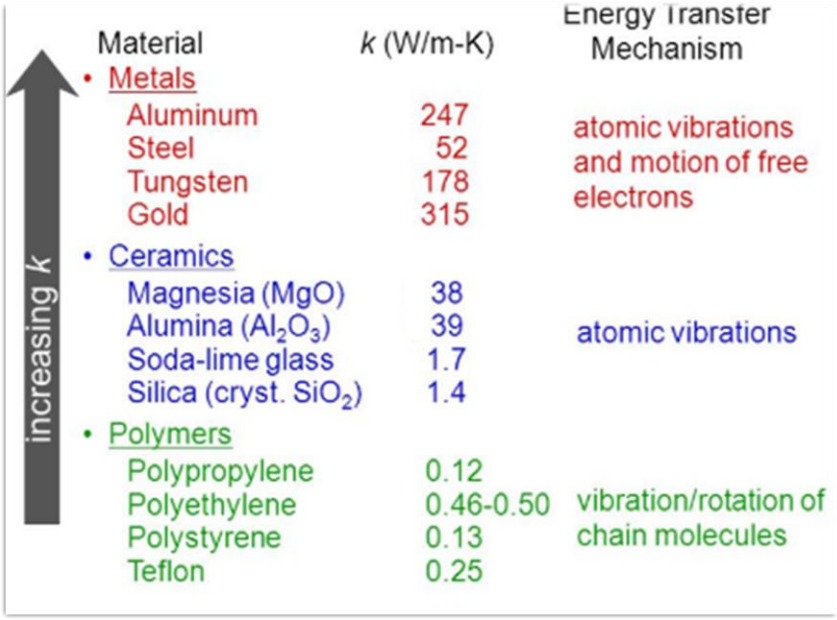

Figure 5 Selected Thermal Conductivity values for some materials [19]

Heat is modeled as vibrational waves, of low frequencies (<100 kHz), referred to as phonons [1]. Therefore, phonons in solids are prescribed by plane waves, which can travel linearly through a continuous path of chemically bonded atoms. It is intuitive to expect that phonons would be strongly affected by the random curvature and sequence of bends along a polymer chain axis considering the plane wave nature of phonons, as shown in Figure 6 [1]. This disordered vibration and rotation of atoms across the polymer chain will cause heat to propagate slower, reducing the thermal

conductivity values for the polymer matrix [5]. As a consequence, phonons in amorphous polymers cannot propagate far; typically, less than 10 nm [20]. Whereas in crystalline structures as metals, heat dissipates faster as a wave across the whole structure, as shown in Figure 6. Therefore, thermal conductivity of metals are much higher than polymer material, as shown in Figure 5.

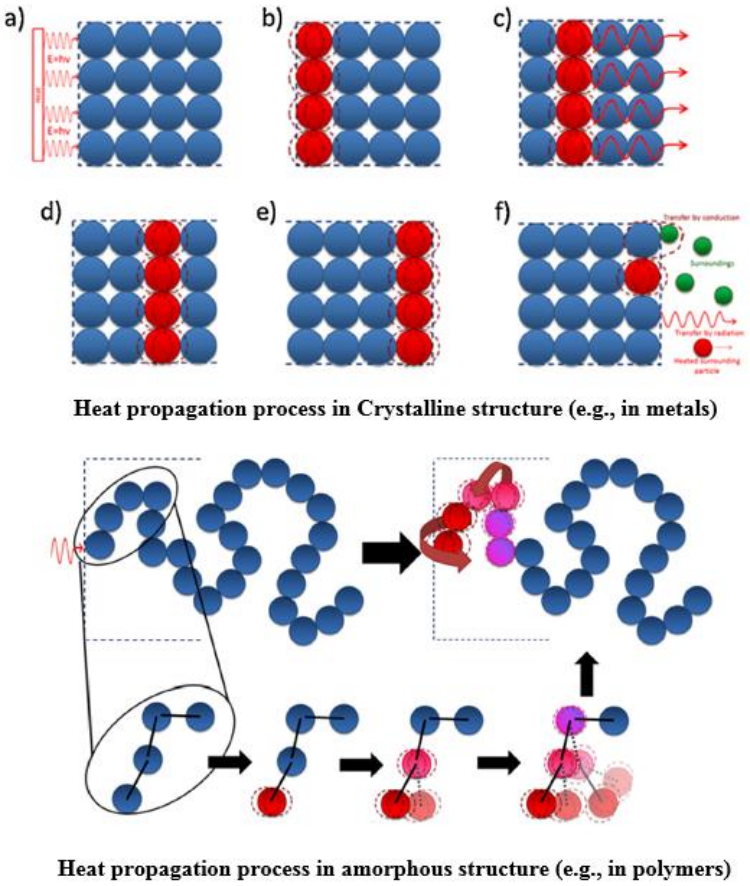

Figure 6 Thermal conduction mechanism in crystalline structures and polymers [5]

Investigators expected to observe a dramatic enhancement in the thermal conductivity of Graphene-based polymer composites after adding high conductive graphene fillers with thermal conductivity of ~3000-5000 W m^{-1} K^{-1} with polymers having a thermal conductivity of ~0.2 W m^{-1} K^{-1} since by the rule of mixing the expected conductivity of the obtained composites should be in the range of ~300 W m^{-1}

K^{-1} for 10 volume % of graphene which was not the case [21,22]. The composite conductivity were instead in the range of 0.3-10 W m^{-1} K^{-1}, which is very low. The issue is that many parameters affect the properties of the Graphene-based composites. After adding Graphene to the polymer matrix, a large number of interfaces are produced, which lead to phonon scattering and the presence of high interfacial resistance called Kapitza resistance [23]. Also, the type and the characteristics of the Graphene used play an important role. Thus, the recommended steps for preparing a polymer composite with high thermal conductivity would be using the right type of Graphene dispersion with the polymer matrix while increasing the number of Graphene pathways through proper orientation of Graphene layers and reducing the resistance between Graphene and the Graphene-polymer interface [3].

2. Electrical Properties

Electrical conductivity in metals is only dictated by the flow of free electrons in the lattice. An electron has to be in the excited level from the filled to the empty state above fermi level E_f for it to become free and charge carrier. In crystalline structures like metals, a large number of free valance electrons are available, and they can be quickly excited to the empty state due to their band structure. Whereas in insulators and semiconductors, the large excitation energy is needed due to the large bandgap [2]. Typical electrical conductivity for polymers is in the range of 10^{-14} to 10^{-17} S/cm [24]. A cluster chains of conductive filler is needed to loosely hold electrons and allow easier delocalization of electrons to improve the electrical conductivity for these polymers [2]. Graphene is one of the most efficient fillers for electrical conductivity enhancement due to its large aspect ratio as simulations and experiments show that fillers with large

aspect ratio lead to better electrical conductivity [25]. Also, the preparation of a 3D interconnected network of Graphene fillers within the insulating polymer matrix has recently emerged as a one another efficient way to improve the electrical conductivity of polymer matrices [17].

3. Mechanical Properties

The impressive mechanical property of graphene by itself is one of the main reasons that make Graphene stand out as original material and as a reinforcing material. This is because of the stability of the sp^2 bond in the hexagonal lattice of Graphene [26]. The mechanical properties of the composites are expected to improve after adding Graphene since the stacking of multiple Graphene layers on top of each other would produce efficient reinforcement. Also, the number of graphene layers plays an essential role in the transfer of the load that takes place from the outer layer to the inner layers of the composite [26]. Young's modulus is expected to increases with the graphene dispersion, mainly in elastomers, because of the significant stiffness contrast between the matrix and the Graphene [18]. In general, the mechanical properties of Graphene-based composites are affected by many parameters, including the type of the Graphene used, the preparation method, the dispersion of Graphene in the matrix, and the orientation of Graphene. Young's modulus and tensile strength, along with the toughness, will dramatically increase even with a minimal weight % of Graphene [26].

E. POSSIBLE APPLICATIONS

Graphene-based polymer composites have the potential to replace metallic components that are typically heavy, rigid, and prone to corrosion with a high thermal

expansion coefficient. The light, conductive, and durable polymer composites can be good candidates in many applications such as wearable/stretchable electronic devices, biomedical devices, batteries, heat sinks, and sensors. [27–31].

1. Electronic Devices

With high electrical conductivity and high carrier mobility (electrons), graphene-based polymer composites can be used in many electronic devices such as electrodes for dye-sensitized solar cells because of their high conductivity [27]. Transparent conducting films that are made from Graphene are usually used in many electronic devices as in solar cells, touch screens, and flat panel display. The flexibility of graphene since it can bend, twist, and roll is one of the most exciting properties of this material. These films are usually made of grown graphene on different substrates using different techniques like Chemical vapor deposition (CVD) and Pulsed laser deposition (PLD). These Graphene-doped conducting polymers have shown better power consumption efficiency than currently available technologies, which make the usage of graphene very promising because of its superior properties [28]. Also, many metallic devices used in aerospace applications like Aluminum are being replaced with high-performance polymers and composites that are lighter, and that can endure harsh conditions available in the outer space. The lightweight of these composites will be one of the primary reasons for the increasingly widespread usage of these materials.

2. Energy Storage

Graphene was applied to lithium-ion batteries (LIB) to improve their performance and sustainability [29]. Song et al. have developed a sustainable cathode

by combining graphene with two promising polymers (poly(anthraquinonyl sulfide) and polyimide) to improve the performance of lithium batteries. Also, graphene and its derivatives were combined with other polymers to be used as a supercapacitor showing a large electrochemical capacitance (210 F g^{-1}) at a discharge rate of 0.3 A g^{-1} [30]. Therefore, graphene can extend the battery's lifetime as well as reduce the charging time while having excellent electrical conductivity.

3. E-textile

Electronic textiles, known as smart fabrics, are wearable cloth with embedded electronics devices in them that come with many functional devices like sensors, LEDs, batteries, and computing devices. These clothes have been increasingly produced because many technologies have been developed, providing an added value for the wearer. This E-textile can be either aesthetic or performance-enhancing, where both categories are both dramatically increasing and affecting both the health and beauty industries. The material used in these E-textile can range from traditional materials like cotton, polyester, and nylon, to advanced and composite materials. The fabrication of Graphene-based polymer composites with high electrical conductivity will be of massive interest in this industry as these composites will sustain the properties of the polymer matrix (flexibility, resistance to corrosion) while being very conductive as shown in Figure 7.

Figure 7 Smart clothing that is electrically conductive embedding a Temperature sensor with a display screen on a winter jacket (Image Source: Thread in Motion)

4. Thermal Interface Materials (TIM)

With the increasing power density of electronic devices as these devices are becoming smaller and smaller, there has been a massive demand for the development of a light thermal interface material (TIM) with very high thermal conductivity for handling the problem of system overheating within different electrical devices [31]. Graphene and its derivatives showed promising results since the thermal conductivity for a single layer of the Graphene sheet is in the range between 3080–5150 W m^{-1} K^{-1} at room temperature, which is the highest of any currently known material [11,12]. So developing a polymer composite with low density and high thermal conductivity will be a breakthrough in electronic devices, as shown in Figure 8, where there was a considerable drop in the temperature of the whole system when filling the gaps with a TIM.

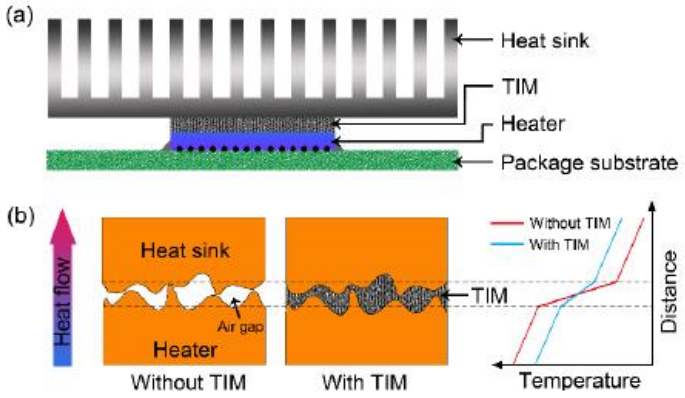

Figure 8 (a) Schematic illustrating electronic devices with interface materials bridging the heater and the heat sink. (b) The functionality of thermal interface materials that help in dropping the temperature when filling out the gaps in electronic devices [31]

5. Biomedical Applications

Graphene-based polymer composites gained an essential role in biomedical applications because of their biocompatibility, physical, chemical, optical, and sensing properties that can be used in many applications. Also, the functionality of Graphene could be improved by adding biodegradable hydrophilic polymers or gels with higher biocompatibility [32]. For instance, Graphene has been conjugated with biocompatible polyethylene glycol (PEG) and chitosan. This composite showed better solubility and stability in physiological solution and has been studied for in vitro drug delivery, imaging, and in vivo photo-thermal therapy for tumors [16]. Also, other Graphene-based hybrid materials were tested and used in tissue engineering, drug and gene delivery, bio-sensing, bio-electronics, and molecular imaging [14,33,34]. As shown in Figure 9, Graphene-based material can be used as transducers for biosensors because of their large surface area, electrical conductivity, and high electron transfer rate [33].

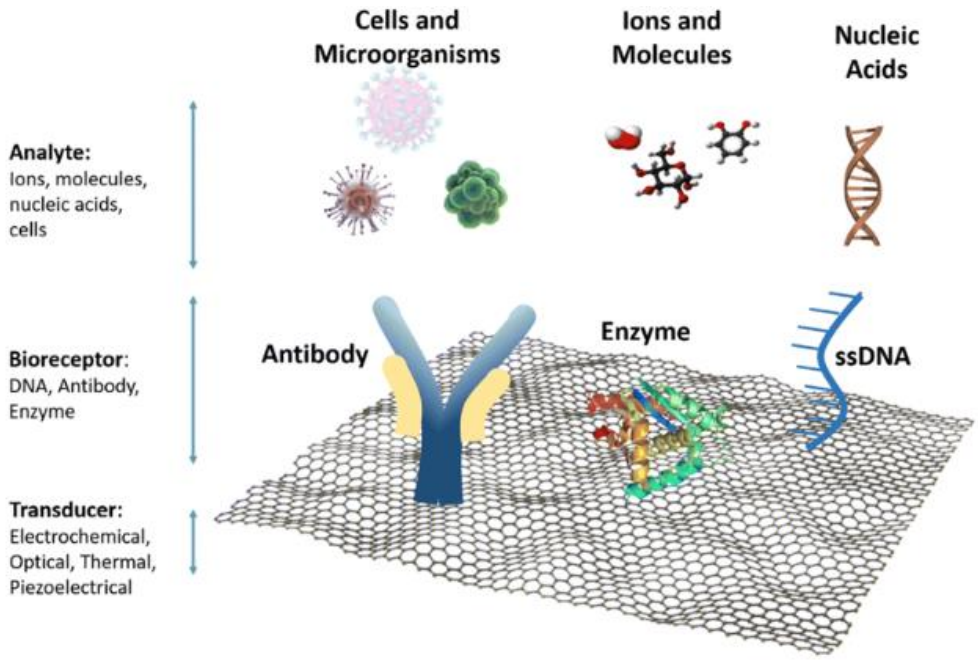

Figure 9 Biosensors and components on a graphene platform [33]

CHAPTER II

REVIEW OF LITERATURE

Over the last decade, researchers used different Graphene derivatives such as Graphene Nano-flakes (GNF) [22], Graphene Sheets (GS) [21], and Graphene Oxide (GO) [35] as fillers to enhance the physical properties (thermal, electrical, and mechanical) of different polymer matrices such as polyethylene (PE) and polyvinylidene fluoride (PVDF) as listed in Table 2. The use of Graphene and its derivatives was after the discovery of the excellent properties of Graphene by itself. For instance, Balandin et al. [10] were the first to measure the thermal conductivity of a single layer of Graphene using Optothermal Ramen technique (OTR), as shown in the schematic in Figure 10a. The high thermal conductivity for a single layer of graphene can reach up 5300 Wm^{-1} K^{-1} due to superior long phonon mean free path [36]. This makes Graphene one of the leading carbon fillers with excellent properties that can be used as a filler in different polymer matrices like PVDF, PE, and PEMAA.

Table 2 Properties of Graphene-based polymer composite materials

Filler material*	Polymer matrix	Filler Content (%)	In-plane Thermal Conductivity (W/mK)	Electrical Conductivity (S/cm)	Fabrication process	Reference
GS@Al_2O_3	PVDF	10 40	0.375 0.586	NA	Solution mixing with ultrasonic dispersion	[37]
FGS/NDs	PVDF	10	0.32	7.1×10^{-7}	Solution	[38]

		45	0.66	1×10^{-7}	mixing followed by ultrasonic dispersion and hot pressing	
GNP	PVDF PE	10 10	1.47 1.84	NA	Solution mixing followed by hot pressing	[39]
GS	PVDF	20	2.06	NA	Solution mixing followed by hot pressing	[21]
GNF	PVDF	10 25	2 10	0.15 0.3	Melt-compression in an L-shape kinked tube	[22]
rLGO	PVDF-HFP	14.2 27.2	14.2 19.5	20 30	Solution casting followed by a low-Temperature chemical reduction process	[35]

Al_2O_3: Alumina coated Graphene sheets; FGS/NDs: Functionalized Graphene sheets with nanodiamonds filler; GNP: Graphene nanoplatelet; GS: Graphene sheet; GNF: Graphene nanoflake; rLGO: Large-area reduced Graphene oxide; PVDF: Polyvinylidene fluoride; PE: Polyethylene.

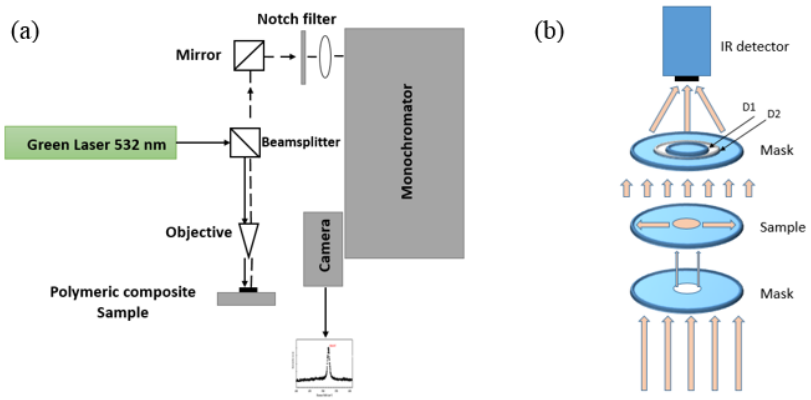

Figure 10 (a) Setup scheme for home-made Raman spectroscopy integrated with laser (λmax =532 nm) (b) Setup scheme for laser flash method to measure in-plane thermal conductivity

Fillers like GS@Al_2O_3 [37], FGS/NDs [38], and GNP [39] were added using different fabrication processes (solution mixing, melt compression, and in-situ polymerization). The use of these fillers was done on different polymer matrices, as shown in Table 2. And because of its high aspect ratio and better dispersion as a 2D material, graphene flakes showed better results in enhancing the properties of Poly(vinylidene fluoride) (PVDF) than other carbon-based materials like CNT, Graphite, and fullerene. PVDF is a typical semi-crystalline polymer with good processing capability, high dielectric constant, and excellent resistance at high temperatures [40]. Yu et al. used solution blending to prepare graphene/PVDF composites, where they succeeded in enhancing the thermal conductivity by two times, reaching a value of 0.45 Wm^{-1} K^{-1} only by adding 0.5 wt% of Graphene filler [41]. Cao et al. showed that Graphene sheets are better than Carbon Nanotubes (CNTs) and fullerene with PVDF at the same loading [21]. The thermal conductivity of Graphene/PVDF reached 2.06 W m^{-1} K^{-1} at a filler loading of 20 wt%, which is an increase of about ten times that of the neat PVDF but was still below the expected value

according to the rule of mixing. However, since graphene is a 2D structure and due to the anisotropic behavior of graphene, aligned graphene composites showed larger conductivity values than unaligned graphene composites. Jung et al. [22] tried to tackle the issue of the proper orientation of Graphene layers along the matrix direction through using melt compression technique in an L shaped tube giving rise to the directional thermal conductivity to approximately 10 W m^{-1} K^{-1} at 25 vol % of GNF in PVDF as shown in Figure 11. This was a considerable improvement in the in-plane thermal conductivity of the graphene/PVDF composite. Also, the electrical conductivity of the obtained composite increased to reach the value of 30 S/m for 25 vol. % of Graphene flakes.

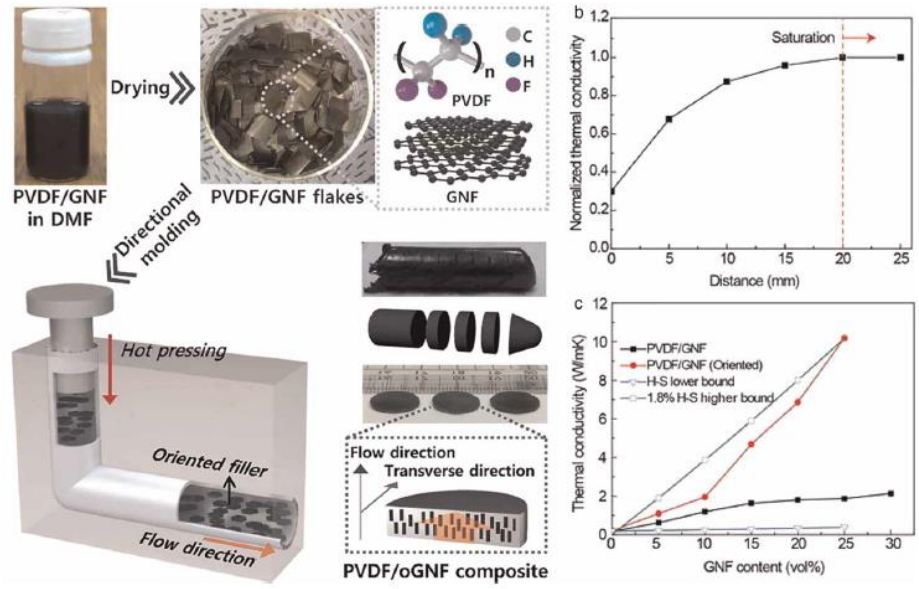

Figure 11 Graphene/PVDF composite preparation process and conductivity values as proposed by Jung et al. [22]

Kumar et al. [35] also achieved a high thermal conductivity (κ) of about 19.5 W m^{-1} K^{-1} for self-aligned large-area reduced Graphene oxide (rLGO) with a content of 27.2 wt % in poly(vinylidene fluoride-co-hexafluoropropylene) (PVDF-HFP). They succeeded in improving the electrical conductivity reaching 30 S/cm for obtained composite films since they used large area reduced Graphene Oxide sheets with smaller inter-sheet contact resistance. Also, they increased the ultimate strength of the polymer to reach 54 MPa for 27.2 wt % rLGO. However, for all the above studies, the filler content used was relatively high (10-30%) to achieve a considerable boost in the thermal and electrical conductivities of the polymer composites. One of the essential advantages of polymers is their low cost, so it is vital that if a high thermal/electrical conductivity composite is developed, the cost remains low, which could be very challenging.

Many models were suggested before to study the thermal conductivity of polymer composites. The useful medium theory was proposed by Garnett in 1904, which approximate the thermal conductivity, as shown in the following equation [44]:

$$\kappa_e = \kappa_m\left(\frac{(p+2)+(p-1)2\varphi}{(p+2)-(p-1)\varphi}\right)$$

Where φ is, the volume fraction and p is the thermal conductivity ratio between the filler and the polymer matrix κ_f/κ_m. This model is a perfect fit with the experimental data for dilute and randomly distributed filler available in a homogeneous mixture where the filler particles have no chemical reactions with the polymer matrix. However, it cannot be applied when the volume fraction of the filler is high, or when the filler has a large aspect ratio as in the case of Graphene, or when there is a large interface between the filler and matrix, or if there is any chemical interaction between the filler and the matrix. A variety of other models were also proposed for different assumptions

about the filler and its distribution in the matrix. Donea [45] used the variation principles to determine upper κ^+ and lower bounding κ^- effective thermal conductivities for composites with spheres:

$$\kappa = \kappa_m(\frac{(p+2)+(p-1)2s}{(p+2)-(p-1)s})$$

$$\kappa^- = \frac{\kappa.\kappa_m}{\kappa_m + (1-\varphi)\kappa}$$

$$\kappa^+ = \varphi\kappa^- + (1-\varphi)\kappa_m$$

$$s = (\frac{a}{b})^3$$

Where a is the radius of inclusion, and b is the largest possible spherical shell that surrounds the inclusion of spherical shells. Also, he used the same procedure to derive an expression for a composite of parallel circular fibers:

$$\kappa = \kappa_m(\frac{(p+1)+(p-1)s}{(p+1)-(p-1)s})$$

It was later determined that the Thermal interface resistance (TIR) between the CNT and the polymer matrix was a dominant resistance that limited the performance of the composite. As a result, efforts to lower the interface resistance and find pairs of polymer matrices and high thermal conductivity fillers with better compatibility became the main focus [1]. For example, Lin, Zhang, and Wong [46] developed a model for a graphite Nano platelet–epoxy composite taking into consideration the orientation of Graphene in the composite:

$$\kappa_{e11} = \kappa_{e22} = \kappa_m(\frac{2+\varphi[\beta_{11}(1-L_{11})(1+cos^2\theta)+\beta_{33}(1-L_{33})(1-cos^2\theta)}{2-\varphi[\beta_{11}L_{11}(1+cos^2\theta)+\beta_{33}L_{33}(1-cos^2\theta)]})$$

$$\kappa_{e33} = \kappa_m\left(\frac{1 + \varphi[\beta_{11}(1 - L_{11})(1 + cos^2\theta) + \beta_{33}(1 - L_{33})(1 - cos^2\theta)}{2 - \varphi[\beta_{11}L_{11}(1 + cos^2\theta) + \beta_{33}L_{33}(1 - cos^2\theta)]}\right)$$

$$\beta_{ii} = \frac{\kappa_{fii} - \kappa_m}{\kappa_m + L_{ii}(\kappa_{fii} - \kappa_m)}$$

$$L_{11} = L_{22} = \frac{p^2}{2(p^2 - 1)} + \frac{p}{2(1 - p^{2^{3/2}})} cos^{-1}p$$

$$L_{33} = 1 - 2L_{11}$$

$$\kappa_{ef} = \frac{L}{2R + (\frac{L}{\kappa_f})}$$

Where $cos\theta$ represents the average orientation of graphite Nano-platelets, and it varies between 1 and 3 for random direction. A strong influence of the aspect ratio and the orientation of graphene sheets is evident. Also, the interfacial thermal resistance (TIR) still plays a significant role in determining the overall thermal transport in the polymer composite. Therefore, studying the thermal conductivity of obtained composites with the parameters that effect this property is one of the main objectives of this project.

In conclusion, none of the researchers above reached ultra-high values for in-plane thermal conductivity or electrical conductivity by using melt compression or solution mixing and casting preparation methods, which allows us to push the boundaries more to define a novel process to achieve polymer composites with enhanced physical properties. Also, none of the researchers above studied the effect of different parameters as the Graphene flake size on the properties of the obtained

composites, which show the importance and the novelty of this project in material's science.

CHAPTER III
GOAL AND RESEARCH OBJECTIVES

In this project, the goal is to prepare Graphene-based polymer composite films with enhanced mechanical properties and ultra-high thermal and electrical conductivity. In the light of previous research work presented in Table 2, the properties of polymer composites can be improved. Presenting a fabrication process and studying the effect of different parameters such as the average graphene flake size, the Temperature, and the polymer used on the properties of obtained polymer composite films are valuable advancements in the field and open doors of opportunities towards new applications as discussed before. These industries need composite materials with high thermal and electrical conductivity and enhanced mechanical properties. Therefore, this research can be divided into the following objectives:

A. Studying the incorporation of Graphene flakes in polymers (PVDF-HFP and PEMMA)

Graphene-based polymer composites can be prepared using a film formation process (i.e., hot mixing of the components in the presence of a solvent, then molding, and solvent evaporation). Therefore, studying the relation and the compatibility between the Graphene used and the polymer matrix is essential. Also, checking the surface morphology of the polymer composite is one of the objectives as these composites should be fully characterized using different techniques that are presented in the methodology section later.

B. Analyzing the Mechanical Properties of obtained composites

As discussed before, Graphene-based polymer composites with enhanced mechanical properties can be used in many domestic and industrial applications (i.e., solar cells, sensors, electronics) that require outstanding material with superior mechanical properties [42]. The objective is to study the mechanical strength and Young's modulus of these films to determine the mechanical properties of the obtained composite films. Also, the effect of graphene flake size on the mechanical properties of these films.

C. Studying the Electrical Properties of obtained composites

Analyzing the electrical conductivity of obtained composites is essential as many factors can affect the conductivity of these composites. In conductive composites and for a random distribution of the filler, a conducting network can form at a specific loading, known as the percolation threshold (x_c). When the filler loading reaches x_c, the electrical conductivity of the polymer composite increases dramatically, and the graph of conductivity versus loading takes the characteristic S-shape, demonstrating the three regimes: insulating, percolating where tunneling starts to happen and conductive as shown in Figure 12. These parameters should be studied and analyzed for obtained graphene-based polymer composites.

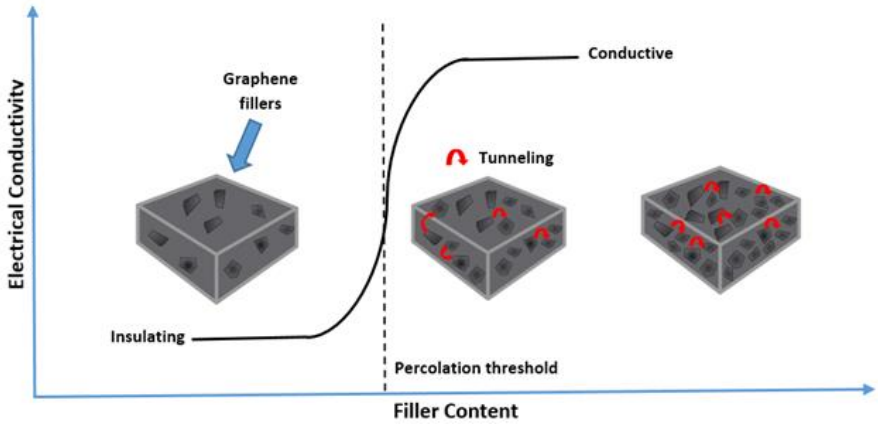

Figure 12 Conduction mechanisms in a composite with increasing filler content [25]

D. Studying the thermal conductivity of obtained composites:

Mixing Graphene that has κ around 3080–5150 W m^{-1} K^{-1} at room temperature with polymer composites with κ in the range of 0.1-0.5 W m^{-1} K^{-1} do not bring the in-plane κ of the polymer composite to the range of ~300 W m^{-1} K^{-1}, not even close. The values were much lower in the range of 2-3 W m^{-1} $K^{-1,}$ which is lower than what is expected, although fillers are expected to be more efficient in transporting heat than polymers itself. In general in any composite, the effective composite thermal conductivity κ_e depends on many parameters like the thermal conductivity of the polymer matric κ_m, the thermal conductivity of the filler κ_f, the thermal interface resistance between the filler and the matrix, the filler loading level, and the particle size, shape, and orientation [1]. Therefore, the thermal conductivity of the composite is some form of a weighted average of the filler and the matrix.

CHAPTER IV
METHODOLOGY

In this chapter, the materials and the methods that were implemented to manufacture the polymer composite films have been fully explained. It is very critical to achieve good dispersion for the Graphene-based filler so that we can enhance the effectiveness of these fillers in the polymer composites and thus achieve high thermal, electrical, and mechanical properties. This is mainly dictated by the preparation method used to fabricate these polymer composites. Also, other parameters may have some effect such as (1) the type of Graphene-based filler used (defect-free Graphene flakes with high purity, Average particle size of the filler, and the aspect ratio) (2) the interfacial interaction between the Graphene-based filler and the polymer matrix (3) the type of the matrix itself.

A. Fabrication of GNF/polymer composite films

Materials: PVDF-HFP copolymer that has an average density of ~1.8 g/mL, and N, N -dimethylformamide (DMF) with density ~0.94 g/mL were procured from Sigma-Aldrich (USA). PEMAA ionomer with 15 wt % methacrylic acid was also purchased from Sigma. In addition to that, three different types of Graphene were purchased: graphene flakes (G1) were purchased from Graphene 3D Lab Inc. (USA) with a purity of 98.5% and specific surface area less than 40 m2/g; Graphene Nano-platelets (G2) Grade M with average specific surface area 120-150 m2 /g and Graphene

Nano-platelets (G3) Grade C, with an average surface area of 750 m2/g were purchased from XGSciences Inc. (USA).

Solution blending or mixing is a widely used method in preparing polymer composites. It is one of the most commonly used methods for the preparation of Graphene-based polymer composites, since it is straightforward, requires no special instruments, and allows for large-scale production. It merely involves dissolving the polymer in a solvent and suspending the filler (Graphene-based filler) in the same or another compatible solvent. Then mixing both solutions according to specific volumes that determine the weight % of the filler in the composite. Then evaporating the solvent to obtain a Graphene-based composite. This process is primarily used with higher molecular weight polymers [47]. Therefore, it is usually a three-step process that includes: dispersing graphene in a suitable solvent (like DMF), vigorous mixing the Graphene solution with the polymeric solution, and finally casting and evaporating the solvent from the mixture to obtain a composite film. During the solution mixing process, high-speed stirring with ultra-sonication can be employed to ensure the proper dispersion of the filler in the composite and to make sure that Graphene fillers are not aggregated in the mixture. After the evaporation, the polymer chains will reassemble, holding the filler together in the composite. The advantage of this method is that the lower viscosity is achieved because of using a solution-based method, which allows us to achieve uniform mixing and dispersion of the Graphene filler within the polymer matrix. The challenges that can happen in this process is that it is sometimes hard to find compatible solvents for the polymer and the filler. One of the significant concerns in solution mixing is the solubility or dispersion of Graphene-based fillers in the

polymer solution. Also, the environmental and economical cost of a large amount of solvent is used during this process that is used in large quantities.

Following tables show the samples code with the volume used for each test of the polymer composites (PVDF-HFP and PEMMA) with the respective graphene content.

Table 3 Recipes for the preparation of GNF/PVDF-HFP composites Paper 1

Sample code ↓	GNF dispersion 5 g/L	PVDF-HFP solution 20 g/L	GNF content wt%
PVDF-HFP-GN0	0	25 ml	0%
PVDF-HFP-GN6	7 ml	25 ml	6.5%
PVDF-HFP-GN10	11 ml	25 ml	9.9%
PVDF-HFP-GN20	15 ml	15 ml	20%

GNF: graphene nanoflake; PVDF: polyvinylidene fluoride; HFP: hexafluoropropylene.

Table 4 Preparation recipes of GNF/PVDF-HFP and GNF/PEMAA composite films using vigorous solution mixing at high temperature and molding in Paper 2

Sample code ↓	**Solvent**	[GNF]	GNF dispersion volume	[Polymer]	Polymer solution volume	GNF content Wt.%
PVDF-HFP-GN10			11 mL		25 mL	9.9%
PVDF-HFP-GN20	DMF	5 g/L	15 mL	20 g/L	15 mL	20%
PVDF-HFP-GN33			20 mL		10 mL	33.3%
PEMAA-GN10			11 mL		25 mL	9.9%
PEMAA-GN20	Toluene	5 g/L	15 mL	20 g/L	15 mL	20%
PEMAA-GN33			20 mL		10 mL	33.3%

GN: graphene nano-flakes; PVDF: polyvinylidene fluoride; HFP: hexafluoropropylene; PEMAA: Polyethylene methyl acrylic acid.

Table 5 Preparation recipes of Graphene-based composite films for three different types of Graphene (G1, G2, and G3) in Paper 3

Graphene types (GN)	Sample name↓	Graphene dispersion [5 g/L]	Polymeric solution [20 g/L]	Graphene content (wt. %)
G1, G2, G3	PVDF-HFP-GN-1	1 ml	25 ml	0.99%
	PVDF-HFP-GN-5	5 ml	25 ml	4.8%
	PVDF-HFP-GN-10	11 ml	25 ml	9.9%
	PVDF-HFP-GN-20	15 ml	15 ml	20%

B. Characterization techniques

The following instruments and techniques were used for characterization of the polymer composites and study their mechanical-thermal properties:

1. Scanning Electron Microscopy (SEM)

The morphological structure of the composite film was investigated by an emission scanning electron microscopy (SEM, MIRA 3 LMU Tuscan, Czech Republic) with an InBeam detector, at an accelerating voltage of 20 KV. The surface morphology

for obtained composites were analyzed using SEM to check the incorporation of graphene flakes in the polymer matrix. Front and cross-sectional SEM images were taken for many composite films to study the dispersion of graphene flakes in the polymer matrix.

2. ATR-FTIR

Cary 630 ATR-FTIR Spectrometer (from Agilent, USA) equipped with a single reflection diamond ATR cell was used for analyzing the surface functional groups of the films for a typical IR spectral range between 600 cm^{-1} and 4000 cm^{-1} at a resolution of 2 cm^{-1}. ATR-FTIR sampling technique was used to enable us to examine samples directly in the solid or liquid state without further preparation methods. Different chemical groups were determined by studying the surface of the composite material obtained. Different information was extracted from the sampling signal of the composite films. Studying the transmission graph for the obtained polymer composite allowed us to conclude the phases with the filler distribution available on the surface of the composite film. The presence of Graphene on the surface alters the peaks that were obtained from the ATR-FTIR for the pure polymer matrix.

3. X-ray diffraction (XRD)

The X-ray diffraction (XRD) patterns of the composite films were carried out using a D8 DISCOVER (BRUKER, Germany) with 2θ ranging from 6° to 60° at room temperature. XRD is a rapid analytical technique that was used for phase identification for crystalline material. It was used to study the structure, composition, and physical properties of obtained materials. Moreover, as discussed before, many features like the

thermal conductivity of crystalline structures are higher than the thermal conductivity of amorphous material. Therefore, it is crucial to characterize the obtained polymer composite films with XRD.

4. Optical Tensiometer

Optical tensiometer (OCA 15EC, DataPhysics, Germany) was used to measure the contact angle of a water droplet on the polymer composite films. A small droplet of water (5 μL) was dispensed and placed directly on the surface of the composite film. The contact angle measurements have repeated a minimum of 10 times for each specimen to get an average for the contact angle for each specimen. Water contact angle (WCA) was measured using an optical tensiometer to study the hydrophobicity of obtained composite films. This will give us an indication regarding the roughness of the obtained surface in addition to the reaction of water with these surfaces, determining if the composite is hydrophilic or hydrophobic. The water contact angle of the composite films was measured using optical tension meter (OCA DataPhysics) (shown in Figure 12). A droplet of pure water (5 microliters) was dispensed and placed directly on the surface of the composite film. A picture was taken at each dispense through a digital camera provided and then analyzed using SCA20 software.

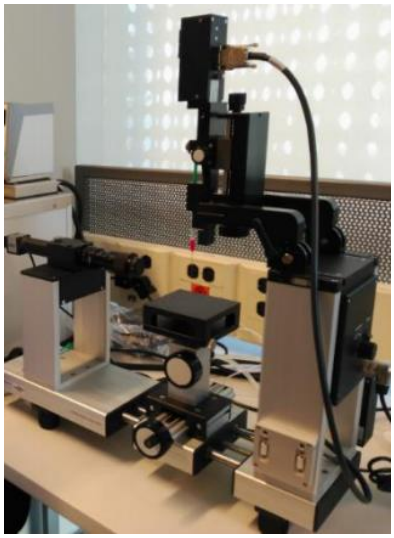

Figure 13 OCA15 Optical Tensiometer

5. Other Equipments:

In addition to that, a thickness gauge (MP1, Brunswick Instrument, UK) with 2 $\times 10^{-3}$ mm resolution was used for measuring the film thickness. TGA Q500 (from TA Instruments, USA) with a responsive low-mass furnace, ultra-sensitive thermobalance, and efficient horizontal purge gas system was used to investigate the thermal stability of obtained composite films. All the measurements were carried out from 20 to 1000 °C at the heating rate of 25 °C /min under nitrogen atmosphere. The initial decomposition temperature (IDT), the maximum weight loss rate (R_{max}), and the temperature at a maximum rate of weight loss (T_{max}) were obtained from the thermograms. The activation energy (E_a) for the decomposition of the film composite was calculated from the TGA thermogram through the integral method based on the Horwitz−Metzger equation [48,49] that is shown below:

$$\ln(\ln\frac{W_0 - {W_t}^f}{W - {W_t}^f}) = \frac{E(T - T_{max})}{R{T_{max}}^2}$$

Where, W_0 and $W_t{}^f$ are the weight remaining at a given temperature, initial, and the final weights, respectively. The heat capacity (c_p) of each sample was measured using a differential scanning calorimeter Q2000 (TA Instruments, USA). The density (ρ) of each composite was calculated as following:

$$\rho = \frac{m}{V}$$

Where m and V are the mass and the volume of the composite film, respectively. The density of each composite was estimated by knowing the density of Graphene (~2.2 g/cm^3) and the polymer (PVDF-HFP has a desnity of ~1-2 g/cm^3), respectively.

The tensile test was performed using Hounsfield HK-100 (China) with a load cell of 1 KN. Each sample (length: 20 mm, width: 10 mm) was placed between the clamps of the machine (Gauge length 15 mm) and then stretched at a controlled extension rate of 2 mm/min until fracture. Elemental analysis for the graphene types was performed using FlashEA 1112 from ThermoFisher Scientific (US). The process includes generating (for a few seconds) very high temperature into the oxidation reactor (~1800 °C), which allows the conversion of the sample to elemental gases that were determined and measured.

For in-plane electrical conductivity, the change in the voltage across the inner two probes was measured when the current passed between the outer two probes. The electrical conductivity for each film was measured using a four-point probe system from Ossila (UK). Electrical conductivity (σ) was calculated using this equation:

$$\sigma = \frac{\ln 2}{\pi}\frac{I}{\Delta V}\left(\frac{1}{d}\right)$$

Where d, I, and ΔV are the film thickness, electrical current, and voltage difference, respectively. Each film was measured 25 times, and the average value with the error was reported for each film. The composite films (Length: 15 mm; Width: 10; thickness: 0.2-0.4 mm) were used for each measurement. In-plane thermal diffusivity of the samples was measured using a laser flash diffusivity analyzer (Netzsch LFA 467 HyperFlash, Germany). A unique sample holder was used for this measurement, and the sample was sandwiched between two circular metal masks. The lower mask had a circular central hole (d0=5 mm) to collimate the laser beam and heat a circular region of the sample. The upper mask had a ring-shaped opening with two concentric circles of (d1=8mm and d2=10mm) to expose the upper surface of the sample to the IR detector. A two-dimensional model was used to correlate the temperature rise as a function of time with inputs of the through-plane thermal diffusivity, sample thickness, laser pulse energy, pulse duration, and geometry of sample holder's openings to determine the in-plane thermal diffusivity [34][35]. The measurements were done on circular samples with a diameter of 15 mm at ~23 °C. The thickness of each sample was measured and defined in the software before each measurement. The reported thermal diffusivity results were the average of 6-8 consecutive measurements. The thermal conductivity (κ) will then be calculated using this equation:

$$k = \alpha \times \rho \times c_p$$

Where $\alpha, c_p,$ and ρ are the thermal diffusivity, the heat capacity, and the density of each sample, respectively. The thermal conductivity enhancement (TCE) that indicates the thermal efficiency of used graphene filler in the polymer matrix is defined by:

$$TCE = \left(\frac{\kappa - \kappa_m}{\kappa_m}\right) \times 100$$

Where κ_m is the thermal conductivity of the polymer matrix. Also, another way for measuring the in-plane thermal conductivity was using Optothermal Raman Spectroscopy (OTR). The OTR is a direct steady-state (independent of time) measurement method where the value of the thermal conductivity of a material is directly measured without any need to calculate the diffusivity, density, or heat capacity of the material tested. Raman spectra for graphene-based polymeric composites were obtained using a homemade setup. The OTR measurements were performed using a green laser with excitation wavelength (λ_{max}= 532 nm), and the power level up to 5 mW. From the obtained Raman signals, the position of the Raman G peak was recorded as a function of the laser power. Due to the increase in laser power (ΔP), the local heating of the sample increases, leading the Raman G peak to shift (Δω). Thermal conductivity κ was calculated by solving the heat diffusion equations in three dimensions across the polymer composite sample. The heat conduction through the surface with a cross-sectional area S was measured from the following heat conduction equation in two-dimensions:

$$\frac{\partial Q}{\partial t} = -K \oint \nabla T . dS$$

Where Q is the amount of heat dissipated over time t and T is the absolute temperature. The exact way for heat propagating through the graphene flake is not fully known, and it depends on the shape of the flake and its boundaries. The radial heat flow from the middle of the flake toward its borders is considered because it is more appropriate as the laser-induced hot spot is much smaller than the suspended graphene flake size. Writing the uniform radial heat flow equation for the two laser excitation power levels P_1 and P_2, which correspond to the two hot spot temperatures, we obtained the expression for the thermal conductivity:

$$K = \frac{1}{2\pi h}\left(\frac{\Delta P}{\Delta T}\right)$$

Where h is the thickness of the Graphene layer, and the local temperature rise ΔT is due to the changing heating power $\Delta P = P_2 - P_1$. Because the excitation power levels are relatively low, the G peak position linearly depends on the sample temperature

$$\omega = \omega_0 + \chi_G T$$

The final expression for the thermal conductivity in the radial heat wave case can be written as:

$$K = \chi_G \frac{1}{2\pi h}\left(\frac{\partial \omega}{\partial P}\right)^{-1}$$

Where ∂ω is a small shift in the G peak position due to the variation ∂P in the heating power on the sample surface. Analogous considerations for the case of the plane-wave heat front lead to the expression:

$$K = \chi_G \frac{L}{2S}\frac{\Delta P}{\Delta T}$$

where L is the distance from the middle of the suspended graphene to the heat sink with the ambient T and S =h × W. Finally, the thermal conductivity can be evaluated as:

$$K = \chi_G \frac{L}{2hW}\left(\frac{\partial \omega}{\partial P}\right)^{-1}$$

CHAPTER V
RESULTS AND DISCUSSIONS

In this chapter, the results that were obtained from different experiments are presented. The first module focuses on the preparation process of graphene based PVDF-HFP composites using solution mixing and molding process and on the enhancement of thermal, electrical, and mechanical properties of these composites. The second module focuses on testing the preparation process with a different polymer (PEMMA) and on the difference between LFA and OTR methods for measuring in-plane thermal conductivity. The third module focuses on the effect of graphene flake size on composite properties. And the fourth module, present the effect of temperature on the thermal, electrical and mechanical properties of obtained composites.

A. Solvent mixing of Graphene Flakes in PVDF-HFP polymer (Based on Paper 1)

1. Characterizations of graphene-based PVDF-HFP composites

The distribution of GNFs on the surface and within the composite films was investigated by SEM (Figure 14). The surface of neat PVDF-HFP-GN0 film is smooth, and the polymer appears to conglomerate in different spherical shapes due to the spherulitic structure of neat PVDF-HFP film [43]. By increasing the concentration of GNF in the composite, more Graphene flakes can be visually detected on the surface of the films. As a result, the roughness of the films increases. We have also observed some defects/voids on the surface of the films, which can be due to solvent evaporation. The distribution of GNFs and PVDF-HFP on the surface of the films seems to be relatively uniform. It seems that the majority of Graphene flakes have distributed horizontally

along the surface, and few small flakes are tilted/broken where the flake edges can be seen across the surface of the composite films. These flake tips that can be spotted at the surface are the reason behind the increase in the cross-plane thermal conductivity after adding GNF to the polymer matrix [22].

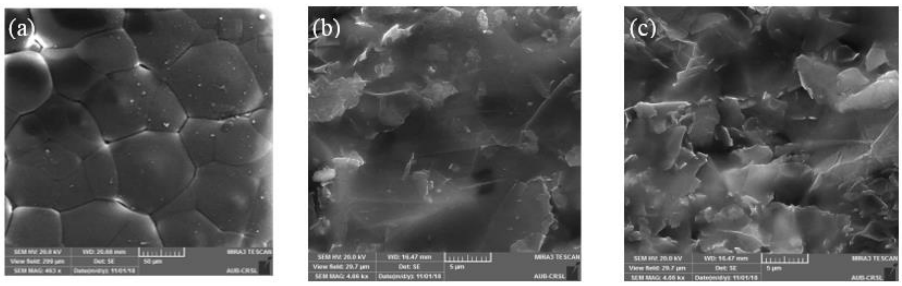

Figure 14 SEM micrographs for molded surface of the composite films obtained for different w.t.% of GNF (a) neat PVDF-HFP (b) 10 GNF w.t.% (c) 20 GNF w.t.% [Colored figure]

Figure 15 shows the cross-sectional view of 20% GNF w.t.% as an example. The GNF layers have stacked on top of each other during the process. The slow evaporation of the solvent (DMF) allows Graphene flakes to settle down slowly on top of each other from the dispersion. Graphene flakes were observed across PVDF-HFP polymer matrix which can be observed in the SEM images in Figure 14. Also, It has been reported that Graphene flakes have a nucleation effect on PVDF-HFP structure, constraining the orientation of the polymer chain and closing the pores across the film [43,51].

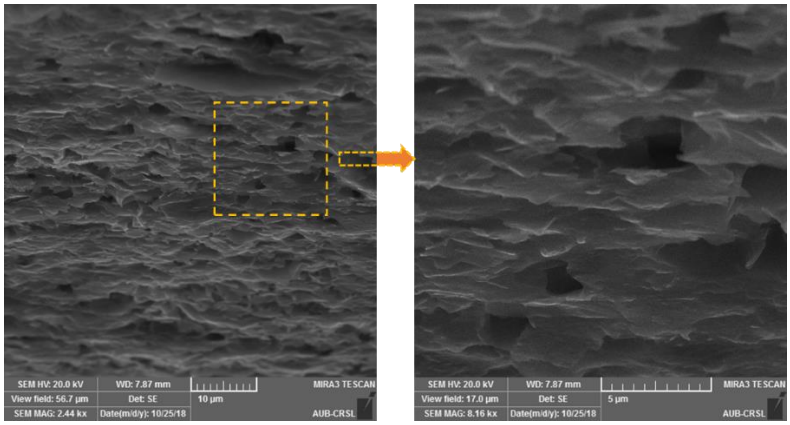

Figure 15 Cross-section scanning electron microscopy images of PVDF-HFP-GN20 at two different magnifications [colored figure].

The ATR-FTIR spectra of the composite films are shown in Figure 16a. The peaks at 760, 790, and 970 cm^{-1} correspond to the α phase structure of PVDF-HFP, and the peaks at 849 and 1270 cm^{-1} correspond to the β phase structure of the copolymer. The peak at 1070 cm^{-1} corresponds to the symmetrical stretching mode of CF_2. Furthermore, The peaks at 1180 and 1400 cm^{-1} correspond to the scissoring and bending vibration of the vinyl group, respectively. These results agree with previous FTIR results reported for neat PVDF-HFP polymer [35,52]. By increasing the concentration of GNFs in the composite films, more Graphene flakes appear on the surface. As a result, the characteristic peaks of the α phase structure of PVDF-HFP diminish, and two representative peaks of Graphene at 2000 and 2200 cm^{-1} emerge, accordingly.

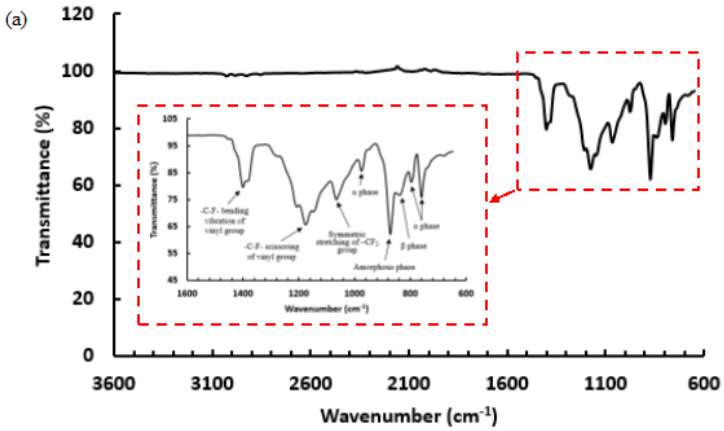

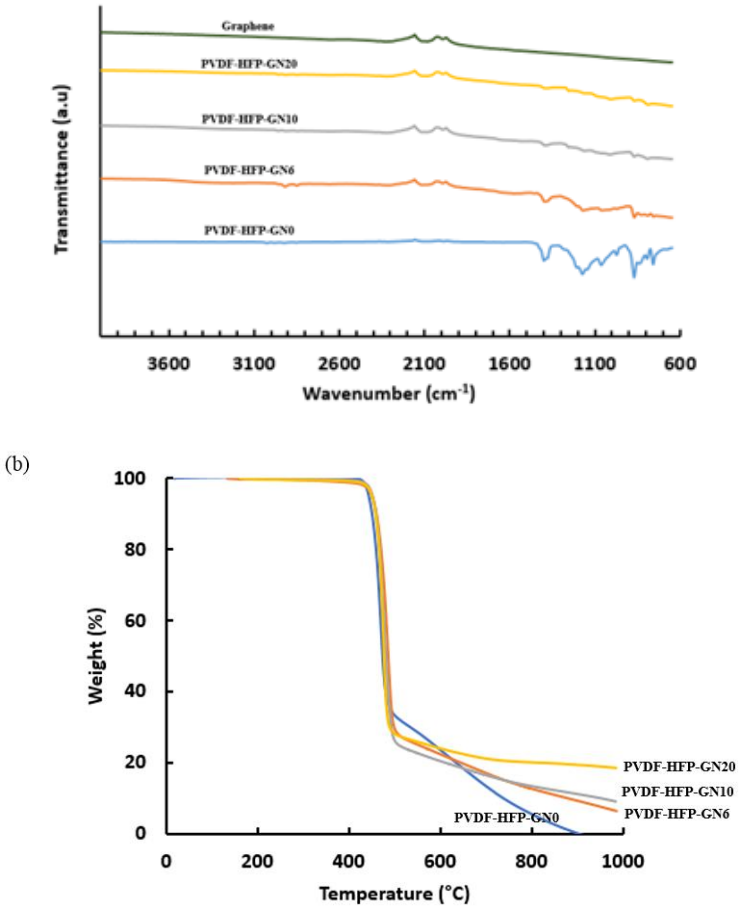

Figure 16 (a) ATR-FTIR analysis for PVDF-HFP and Graphene composite films (b) TGA of GNF/PVDF-HFP composite films under N2 atmosphere

Polymer composites with excellent thermal stability are required in many applications (e.g., electronic devices, insulators) [5]. Therefore, TGA was used to understand the thermal stability of neat PVDF-HFP and GNF/PVDF-HFP composite films (Figure 16b). The values of IDT, T_{max}, R_{max}, and E_a were obtained from the thermographs and are reported in Table 4. IDT indicates the apparent thermal stability of the composite film, i.e., the failure temperatures of the composite in processing and molding, and is determined from the onset of weight loss of the sample in the TGA thermogram.

The degradation profiles of these films were almost similar with IDT at 440-450 °C. PVDF-HFP melts at 155°C without losing any weight till 440°C [53,54]. This indicates that the interaction of Graphene flakes with the polymer matrix is not changing the degradation profile. The PVDF-HFP sample was completely decomposed above 900 °C (i.e., 100% weight loss). In contrast, the carbon ash remaining varies between each of the samples, depending on the original GNF content (%) in the polymer matrix. Also, the activation energy (Ea), which is a measure of the energy barrier that material must overcome to undergo structural reorganization or motion, increases as the w.t.% of GNF increases in PVDF-HFP as shown in Table 4. The presence of Graphene flakes impedes the movement of the copolymer PVDF-HFP chain, increasing the composite crystallization activation energy [55,56].

Table 4 Thermal stability and degradation data of the composite films from TGA under Nitrogen Atmosphere

Test Composite	IDT[a] (°C)	T_{max}[b] (°C)	R_{max}[c] (%/°C)	E_a[d] (kJ/mol)
PVDF-HFP-GN0	442	462	-1.85	329
PVDF-HFP-GN6	447	481	-2.03	348
PVDF-HFP-GN10	449	482	-2.31	450
PVDF-HFP-GN20	449	483	-2.36	476

[a]IDT: Initial decomposition Temperature; [b]T_{max}: Temperature at the point where the maximum rate of weight loss occurs; [c]R_{max}: the slope of weight loss at T_{max}; [d]E_a: activation energy for the decomposition of cured GNF/PVDF-HFP composite films.

2. Mechanical properties:

Figure 17 shows that by increasing the concentration of GNF in composite films, the mechanical properties improve. This increase can be related to several factors: (a) the proper distribution of the Graphene flakes in the polymer matrix (PVDF-HFP) [43], (b) the stacking of multiple Graphene layers on top of each other producing an efficient [26], (c) the uniform dispersion and orientation of Graphene flakes in the polymer matrix that improves the mechanical properties of the composite films [35]. Graphene flakes restrict the segmental movement of the polymer chains causing the Young's Modulus to be improved accordingly, as shown in Figure 17b [57]. Further increase in the Graphene content did not produce significant changes because the films with higher GNF concentrations (>25%) were all very brittle and had poor mechanical properties (data not shown in Figure 17) since increasing Graphene filler loading cannot always provide significant improvement due to brittleness of Graphene itself [58]. By adding 6 w.t.% GNF to the composite film, the tensile strength of the film increased from 15 MPa to 30 MPa (i.e., 100% enhancement) and Young's modulus measured at 3% strain rate increased from 287 MPa to 427 MPa (i.e., 49% enhancement). These graphene-based composite films showed excellent elongation at break when the weight % of graphene flakes was lower than 20%. Composites with such tensile strength and tensile strain can be used in many applications that require flexible material [59].

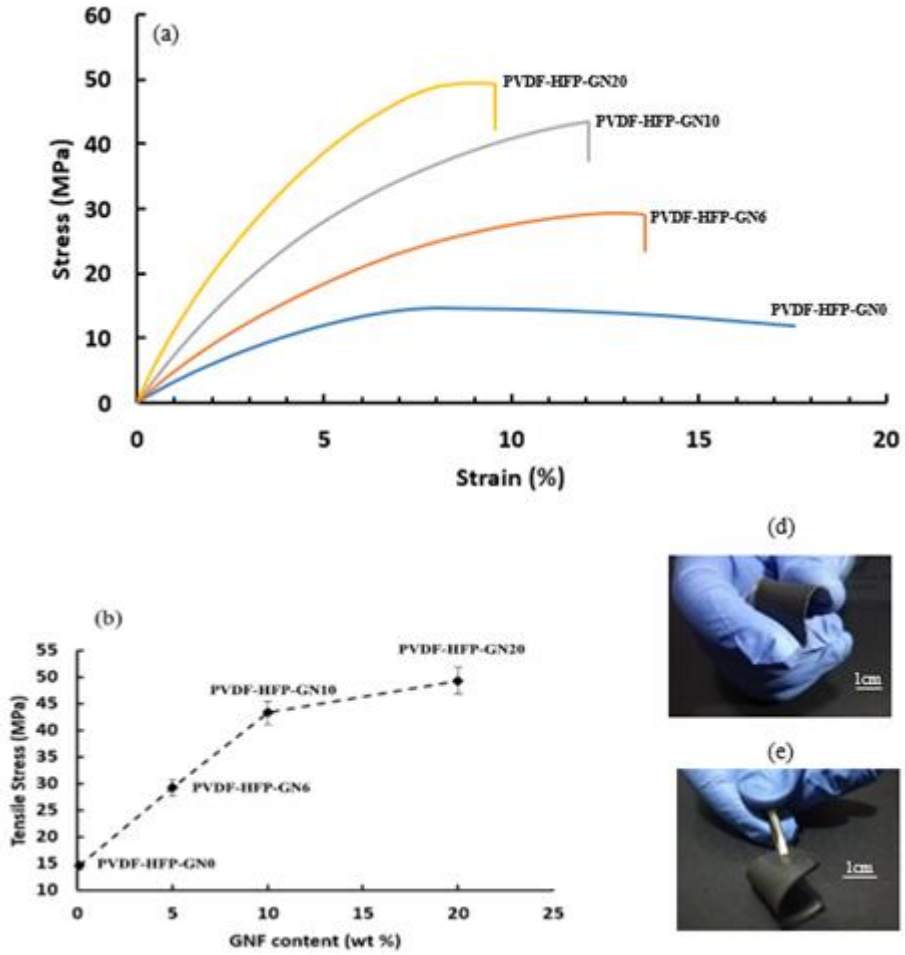

Figure 17 (a) Stress-strain curves of the composites (b) The enhancement of the tensile strength and Young's modulus as a function of GNF content in the composites (d and e) two photographs showing the flexibility of PVDF-HFP-GN20

3. Thermal conductivity

Figure 18 demonstrates the increase in thermal conductivity (κ) as a function of GNF content. As an example, the thermal diffusivity (α), the density (ρ), and the heat capacity (c_p) for PVDF-HFP-GN6 were 4 mm^2/sec, 1.78 g/cm^3, and 1.1 J/g°C, respectively. The thermal conductivity (κ) was calculated to be ~8 W m^{-1} K^{-1} for this composite, which is 36 times larger than that of the neat matrix (0.22 W m^{-1} K^{-1}). PVDF-HFP-GN20 exhibited a very high thermal conductivity of ~25 W m^{-1} K^{-1}, which is a record for Graphene-based composite films compared to the values reported in the

literature till now (Table 2). These high thermal conductivity values can be attributed to increasing thermal transport capacity due to the alignment of Graphene layers across the composite film. Proper orientation of the Graphene flakes within the composites would provide a path of lower thermal resistance for phonon travel. This transport is not only in-plane but also cross-plane for the composite films, as reported by Jung et al. [22]. The vertical bridging between different Graphene layers that were shown in the SEM in Figures 14 & 15 may explain the improvement of the thermal conductivity of the composite films in the cross-plane direction. A linear empirical formula was found with high regression value (R^2>0.97) for the thermal conductivity as a function of GNF content. As the GNF content increases, Graphene flakes tend to overlap, as shown in the SEM images in Figure 14 for sample PVDF-HFP-GN20. This linear trend shows that by adding more Graphene, Graphene layers with lower thermal Kapitza resistance will be produced because of the proper orientation and integration between Graphene and the polymer matrix (PVDF-HFP) allowing phonons to be transported while being less scattered across the boundaries [5] (Figure 19).

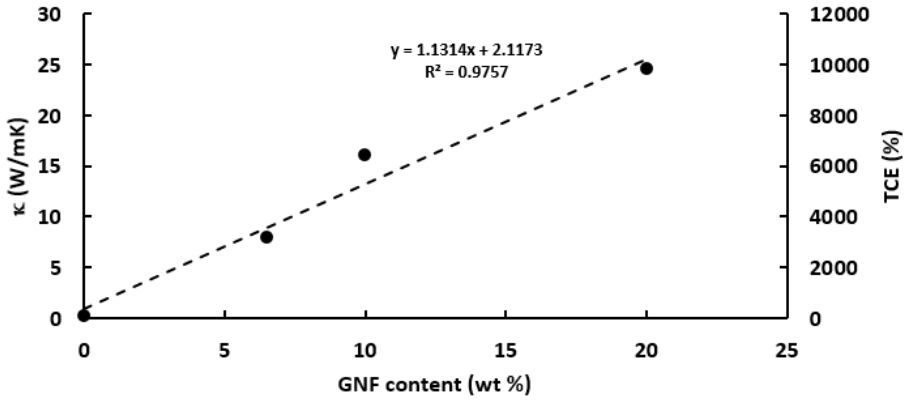

Figure 18 Thermal conductivity and Thermal conductivity enhancement as a function of GNF w.t. %

This enhanced thermal conductivity can also be attributed to the characteristics of Graphene flakes used in the process (i.e., purity of 98.5%, minimum defects, Aspect ratio). Only Graphene flakes were used, not Graphene oxide (GO), which can have some defects or impurities that can cause some scattering for phonons across the matrix [6]. Furthermore, this may be the main reason that made this process more effective than other processes reported before [7,35]. Also, the sizeable interfacial contact area of Graphene, as well as the strong interface coupling between GNF/PVDF-HFP, helped in creating multiple thermal pathways across the polymer composite films. As can be seen in Figure 14, GNFs are well dispersed in the PVDF-HFP matrix via vigorous solution mixing, molding, and solvent evaporation process. This functional integration between Graphene and the polymer allows phonon to transport across the composite film, allowing heat to propagate quickly. The whole process of phonon propagation with the movements of electrons across tilted and aligned Graphene layers is represented in the scheme in Figure 19. Out of plane thermal conductivity were not meaured for the composite films obtained, only in-plane thermal conductivity were measured. Also piozoresistivity for the composites were not studied but this can be a topic of a future study. When some of the atoms in each graphene layer come into contact with a heat source and begin to vibrate, phonons will quickly pass to the surrounding atoms by the strong force of the covalent bond [60]. Proper alignment and orientation of Graphene Layers in the composite films decrease Kapitza resistance and boundary phonon scattering establishing a thermal pathway in the polymer matrix, which allows phonons to transport more efficiently.

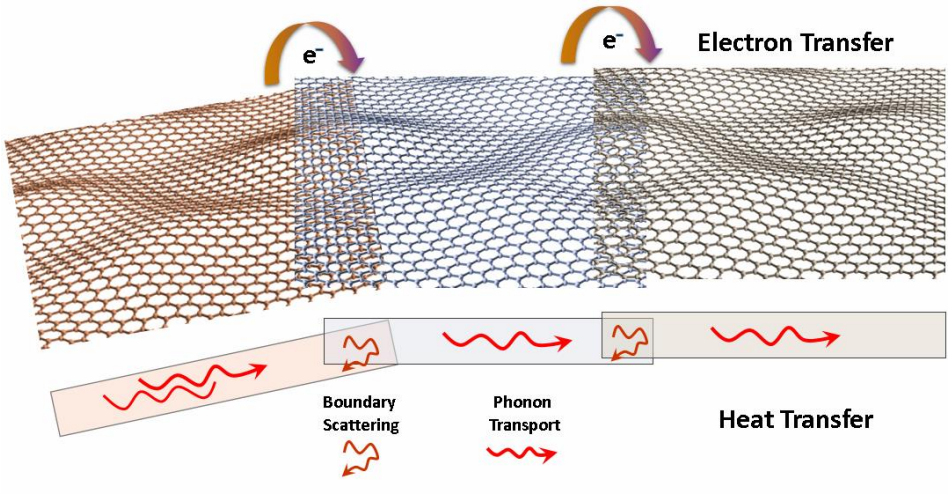

Figure 19 A scheme showing the transport of electron and phonon across the tilted and aligned Graphene layers within the GNF/PVDF-HFP composites

B. Comparison Analysis between laser flash and OTR methods (Based on Paper 2)

In this module, the solution mixing and molding process that was used for the incorporation of graphene Nano-flakes in Poly(vinylidene fluoride-co-hexafluoropropylene) (PVDF-HFP) was tested with a copolymer (poly(ethylene-co-methacrylic acid) copolymer (PEMAA). The orientation and stacking of graphene Nano-flakes were confirmed using a scanning electron microscope (SEM). The thermal conductivity values for these composites were obtained using: (a) laser flash method (commercially available), and (b) an Optothermal Raman technique (homemade device). As discussed before, the OTR method measures the in-plane thermal conductivity directly from the relation between the excitation power and the position of the Raman resonance. The data obtained from Raman spectroscopy were analyzed, assuming heat propagation in three-dimensions and two-dimensions. The Raman results obtained based on the two-dimensional model were very close to the results obtained

using the laser flash method with less than 10% difference. The Optothermal Raman spectroscopy was found to be a promising technique for measuring the in-plane thermal conductivity of carbon-based polymer composites. PVDF-HFP and PEMAA composite films with very high in-plane thermal conductivity (25 W $m^{-1}K^{-1}$) were obtained through the incorporation of graphene Nano-flakes (20% wt. concentration). Considering a very low thermal conductivity of these polymers (less than 0.2 W $m^{-1}K^{-1}$), this corresponds to a significant enhancement of roughly 12400%.

Over the last decades, researchers tried to use different techniques to measure the thermos-physical properties of these materials, whether in 3D bulk form or thin-film form with a broad temperature range. Transient hot-wire technique and laser flash method were widely employed to characterize 3D bulk materials, whereas Optothermal Raman (OTR) spectroscopy and 3ω method were used for thin-films characterization [12]. These methods could also be divided into contact resistive and non-contact optical categories [13]. Researchers prefer direct, non-contact, and non-destructive methods like laser flash diffusivity method and OTR spectroscopy to measure the thermal conductivity values for different materials [14–16]. However, the research papers that compare the results from these measuring techniques are far from sufficient. Raman spectroscopy was used to measure the thermal conductivity of a three-dimensional system of low thermal conductivity and proved efficient for measuring the thermal conductivity of these films [14–16]. Also, Graphene has an exceptional Raman signal where G peak and $2D^*$ band exhibit strong temperature dependence [14]. These reasons allowed Balandin et al. [4] to use these features to measure the thermal conductivity of a single layer of graphene using OTR spectroscopy. In OTR spectroscopy, the Raman Spectrum is used as a thermometer to calculate the temperature increase in graphene in

response to the heating process done by the laser [17]. The position of the Raman G peak of Graphene depends on the local temperature, and its Lorentzian shape allows exact measurements [18]. Before, calibration measurements should be done to plot the shift in the G peak position as a function of graphene's temperature that was imposed externally [18].

Not like the laser flash method, OTR spectroscopy does not require separate experiments to measure the heat capacity and density of the material tested, which may cause an accumulation of uncertainties and lead to more substantial errors. Malekpour et al. [17] used OTR spectroscopy to calculate the thermal conductivity of polyethylene terephthalate (PET) substrate coated with Graphene laminate where this coating increased the thermal conductivity of the polymer by 600 times. Yan et al. [19] used OTR spectroscopy to measure the thermal conductivity of monolayer of Molybdenum Disulfide (MOS_2) that has a temperature-dependent Raman spectrum in the Temperature range of 100–320 K solving a two-dimensional heat dissipation equation. Also, Peimyoo et al. [20] reported the thermal conductivities of the monolayer (1L) and bilayer (2L) Tungsten disulfide (WS_2) that was grown using chemical vapor deposition (CVD) via OTR spectroscopy. Similarly, Yan et al. [21] used Raman measurements to study the phonon and thermal properties of exfoliated tantalum diselenide (2H-$TaSe_2$) thin films. Besides, Lue et al. [22] used micro-Raman spectroscopy to measure the anisotropic in-plane thermal conductivity of suspended few-layers of black phosphorus. However, none of the researchers above did a detailed analysis where they compared a laser-flash method with the OTR spectroscopy method, creating a consensus around the thermo-physical properties of designed three-dimensional Graphene-based polymeric

composites, including thermal conductivity values, which define their thermal transport abilities.

To the best of our knowledge, the OTR spectroscopy method has not been used yet for measuring the thermal conductivity of bulk 3-D graphene-based PVDF-HFP and PEMAA polymeric composites, which shed light on the importance of this test. Most of the amorphous polymers have a very low thermal conductivity, which is lower than 0.5 $W\ m^{-1}K^{-1}$, which can limit their functionality in many applications. PVDF-HFP is widely applied in filtration, ionic conductivity, and wastewater treatment due to their excellent mechanical properties, chemical stability, and remarkable piezoelectric and ferroelectric properties [43]. PEMAA is one of the exciting ionomers with unique self-healing behavior that can be used in many industries [61]. So it is essential to enhance their thermal properties so that they can be used in different applications that require materials with high in-plane thermal conductivity values. Therefore, reporting a manufacturing process to fabricate high conductive polymers is considered a breakthrough. The in-plane thermal conductivity of these conductive films was measured using OTR spectroscopy and laser flash techniques for validation and comparison, which was not done before in any previous research.

The Raman spectrum for pure Silicon was obtained by the setup first to standardize our home-made OTR apparatus, and the result was similar to the spectrum obtained by other Raman measuring methods [62]. The sharp peak that characterizes Silicon was seen at $\sim 520\ cm^{-1,}$ as shown in Figure 20. Therefore, no extra shifts existed in the setup because of the well-known sharp peak of Silicon at $\omega = 520\ cm^{-1}$.

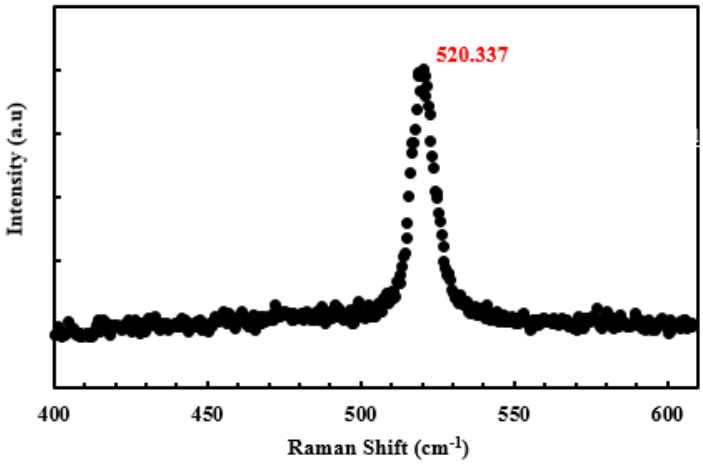

Figure 20 Raman Spectrum of a Silicon wafer obtained with a sharp peak at ~520 cm^{-1}

Our Raman measurements for graphene-based polymeric composites demonstrated that the shift of the G peak is very sensitive to the heating laser power, which makes the thermal conductivity values for these composites measurable. First, we tried to retrieve the thermal conductivity of the measured samples by considering that the heat propagates uniformly in a three-dimensional system. In that case, the thermal conductivity can be calculated from $K = {2\Delta P}/{\pi a \Delta T}$, where a is the diameter of the heating spot, ΔP is the variation of the power on the sample, and ΔT is the variation of the local temperature, which can be obtained by calibrating the Raman shift [63]. However, the results strongly disagreed with those obtained by laser flash measurements indicating that the model of three-dimensional heat propagation in the measured samples is inadequate. Then, we considered that the heat propagates only in the two-dimensional graphene flakes. With the two dimensional-model, the results obtained by Raman spectroscopy showed satisfactory agreement with the results obtained by the laser flash measurements. This can be understood if we realize that in the case where the thermal conductivity of the matrix is very low (~0.2 $Wm^{-1}K^{-1}$ for PVDF-HFP and PEMAA), the heat will only propagate in-plane across the graphene

Nano-flakes that are distributed and stacked on top of each other along with the polymer matrix. Therefore, to obtain the in-plane thermal conductivity, the heat diffusion equation is only needed to be solved in two-dimensional geometry. Moreover, because of the dark appearance and substantial thickness of the composite films, the total laser power will be entirely absorbed by the samples.

Figure 21 shows the D and G peaks for PVDF-HFP-GN33 at 5 mW laser power. Two Gratings (600 and 2400) were used with a resolution of 0.3 cm^{-1} to precisely locate the G peak in the Raman Spectrum of PVDF-HFP-GN33, which was found to be located at ω =1580 cm^{-1}.

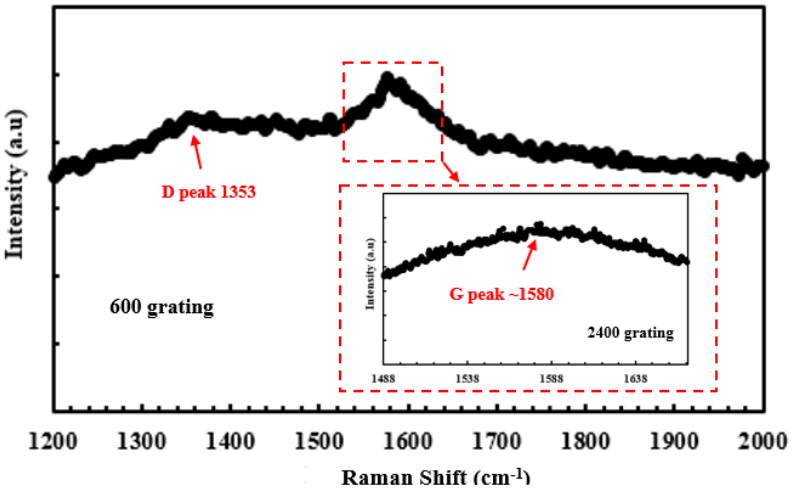

Figure 21 Raman Spectrum of Graphene-based polymeric composite PVDF-HFP-GN33 under 5 mW laser power

Reducing the laser power from P_1= 5 to P_2=4 mW, the G peak in the Raman spectrum of PVDF-HFP-GN33 shifted from ω_1 =1580cm^{-1} to ω_2 =1582 cm^{-1}. The solution of the heat diffusion equation in two-dimensions was used to calculate the thermal conductivity of the Graphene-based polymeric composite [10]:

$$\kappa = \chi_G \frac{L}{2hW} \left(\frac{\partial \omega}{\partial P}\right)^{-1}$$

κ is the thermal conductivity value of the composite film χ_G is the slope of the calibration curve of the frequency shift to the power shift that was found to be $\chi_G = -0.016$ $cm^{-1}\,K^{-1}$ for Graphene by Balandin et al. [10]. L is the length from the center to the end of the graphene flake, h is the thickness, and W is the width of the Graphene Nano-flake. These values were extracted from the datasheet of the Graphene Nano-flakes obtained from the supplier Graphene Laboratories Inc. (USA) where $\frac{L}{W} = 0.5$, h=60 nm , and $\frac{\partial\omega}{\partial P} = \frac{\Delta\omega}{\Delta P}$ is the ratio of the shift in G peak position with respect to the change in the power of the laser.

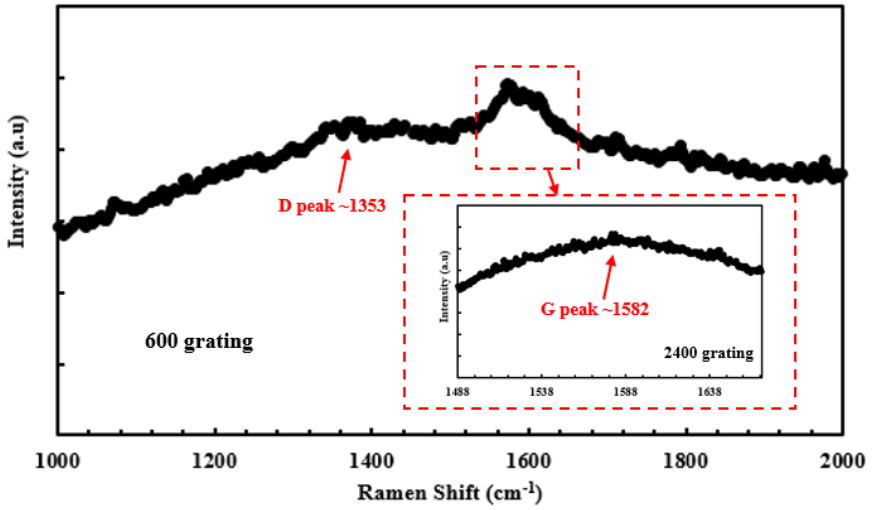

Figure 22 Raman Spectrum of Graphene-based polymeric composite PVDF-HFP-GN33 under 4 mW laser power

Therefore, for PVDF-HFP-GN33 sample, the in-plane thermal conductivity was obtained using the above equation:

$$\kappa = 37.7 \pm 5.3\ W/mK$$

The value calculated was compared with the value obtained for in-plane thermal conductivity with the laser flash method for PVDF-HFP-GN33. The value reported for thermal diffusivity was α=15.8 mm^2/s, and the specific heat capacity measured by DSC

was c_p=1.25 J/g.°C. The density of the sample was ρ= 1.9 g/cm^3. Therefore, the in-plane thermal conductivity using the laser flash method was also calculated:

$$\kappa = 38 \pm 0.2\, W/mK$$

Similarly, all Raman graphs for PVDF-HFP-GN33 were obtained at different laser powers, and the shift of the G peak is shown in Figure 23 below.

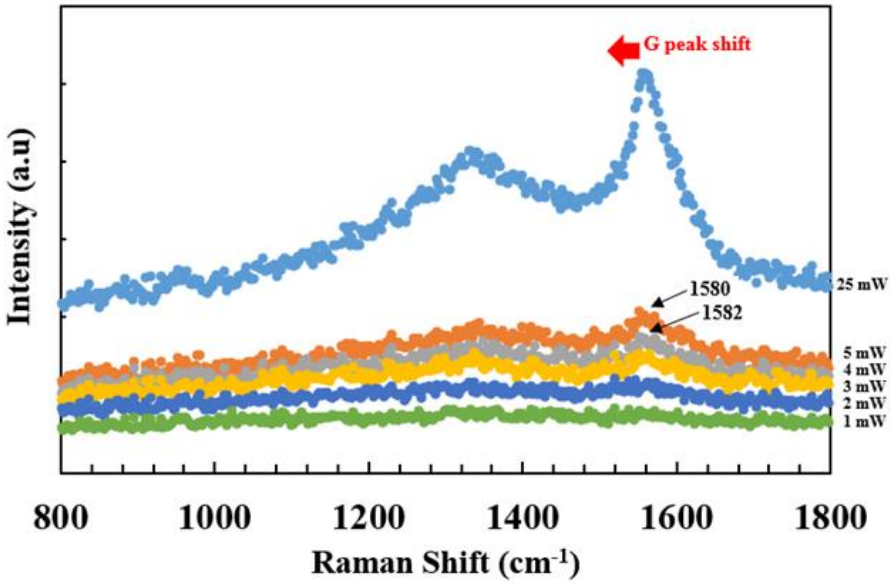

Figure 23 G peak shift in the Raman Spectrum of Graphene-based polymeric composite PVDF-HFP-GN33 at different laser powers (25,5,4,3,2,1 mW)

Raman Spectrum for PVDF-HFP-GN10 and PVDF-HFP-GN20 were also obtained, and the shift in the G peak between two laser powers P_1 =5mW and P_2 =3mW is shown in Figure 24.

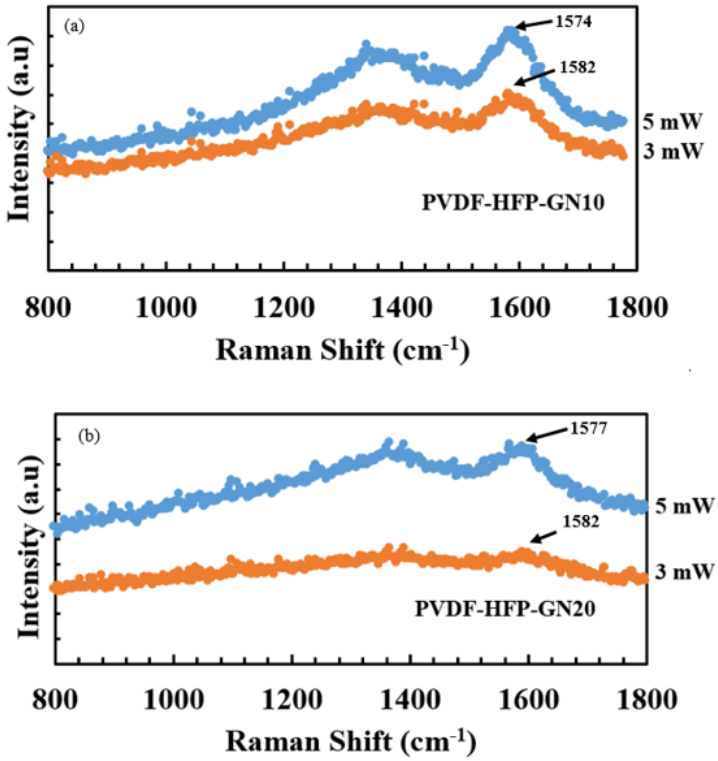

Figure 24 The Raman Spectrum of PVDF-HFP composites (a) PVDF-HFP-GN10 (b) PVDF-HFP-GN20 at 5 mW and 3 mW laser power

The Raman G peak shift was recorded in response to the change in the laser power ΔP, and the in-plane thermal conductivity was calculated using the two-dimensional heat propagation model. Also, the thermal diffusivity for PVDF-HFP-GN10 and PVDF-HFP-GN20 composites was measured using the laser flash method. The thermal diffusivity was found to be $\alpha_{10\%GNF} = 7.85 \pm 0.13\ mm^2/sec$ and $\alpha_{20\%GNF} = 10.67 \pm 0.12\ mm^2/sec$. The in-plane thermal conductivity values of the composite increased dramatically after adding graphene Nano-flakes to the polymer matrix. Due to the proper arrangement and alignment of these graphene Nano-flakes as confirmed in SEM images, heat dissipated quickly as these graphene Nano-flakes established a very conductive thermal pathway in the polymer matrix as reported by the authors in previous work [36]. The same analysis was done on PEMAA polymeric

composites, as shown in Figure 25. Raman G peak shift was measured after changing laser power between P_1 =5 mW and P_2 =3 mW, and a two-dimensional heat propagation model was used to calculate the in-plane thermal conductivity for PEMAA-GN10, PEMAA-GN20, and PEMAA-GN33.

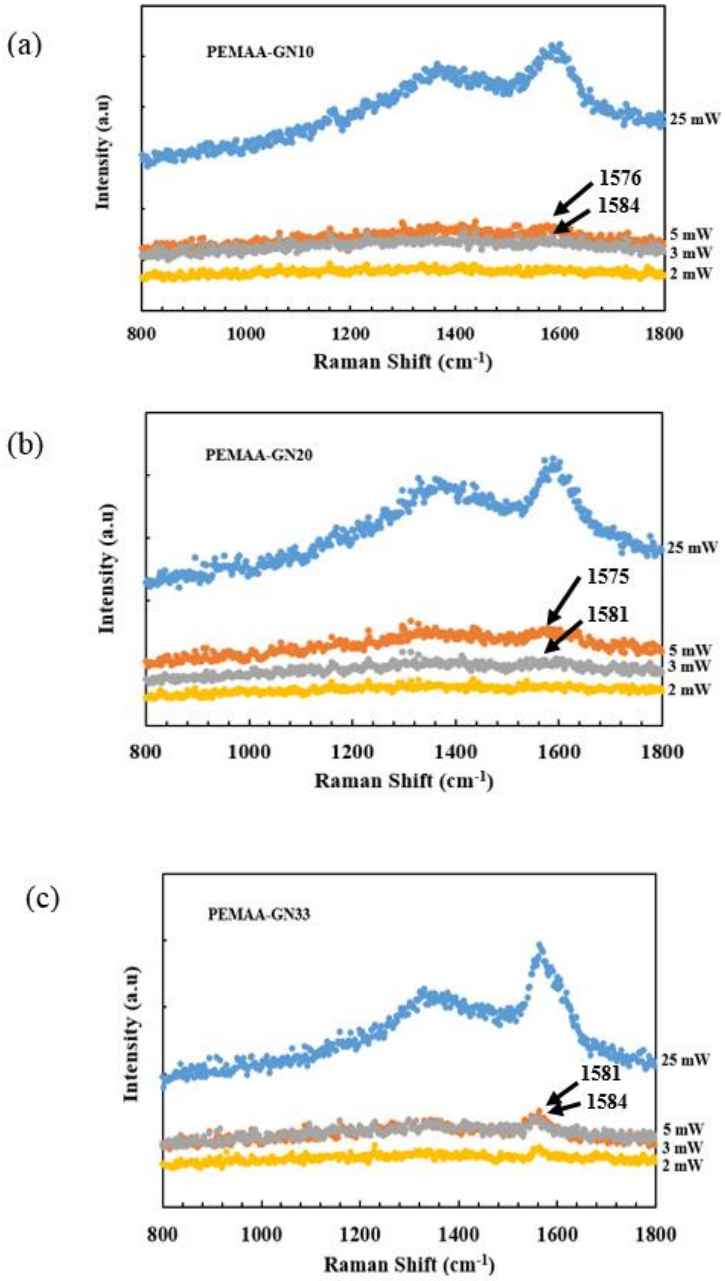

Figure 25 The Raman Spectrum of PEMAA composites (a) PEMAA-GN10 (b) PEMAA-GN20 (c) PEMAA-GN33 using different laser powers (25,5,3,2 mW)

The thermal diffusivity for PEMAA polymeric composites was obtained using the laser flash method. The values were $\alpha_{10\%GNF} = 6.48 \pm 0.09\ mm^2/sec$, $\alpha_{20\%GNF} = 11.18 \pm 0.20\ mm^2/sec$, and $\alpha_{33\%GNF} = 18.90 \pm 0.27\ mm^2/sec$. Table 6 summarizes the values obtained by OTR spectroscopy compared to the laser flash method for both copolymers PVDF-HFP and PEMAA. The obtained values were very close for both polymers with less than 10% difference for different graphene Nano-flakes weight %. This result promotes OTR spectroscopy as a powerful direct technique for measuring the in-plane thermal conductivity of 3D graphene-based polymeric composites where heat only propagates in-plane across the graphene Nano-flakes. Also, the results for in-plane thermal conductivity continued the work done in the first module [36] and showed that very high values were obtained by adding graphene Nano-flakes to different polymeric composites (PVDF-HFP and PEMAA) using the process of vigorous solution mixing, then pouring the mixture into a mold, and leaving the solvent to evaporate slowly. This proper orientation and alignment of graphene Nano-flakes enhance the thermal properties of obtained composites allowing heat to propagate quickly within these thermal channels that were created in the composite films after adding graphene Nano-flakes to the polymer matrix that have very low in-plane thermal conductivity.

The Graphene-based polymer composites showed very high values of in-plane thermal conductivity, ~16 to ~43 (W/mK), which is much larger compared to the thermal conductivity of PVDF-HFP and PEMAA, ~0.2 (W/mK). Therefore, the in-plane thermal conductivity of these composites was enhanced 80 -214 times. This corresponds to a 7900- 21000% increase in the in-plane thermal conductivity of the produced polymeric composites.

The in-plane thermal conductivity values measured by LF and OTR spectroscopy techniques were very close to each other, and we observed a linear correlation between in-plane thermal conductivity and the graphene flake content as shown in Figure 26.Therfore, OTR spectroscopy technique can successfully be used for measuring the in-plane thermal conductivity of graphene-based composites directly by knowing the average size of graphene flakes within the composites.

Table 5 In-plane thermal conductivity values obtained using laser flash and Raman technique for graphene-based composites: GNF/PVDF-HFP and GNF/PEMAA

	Laser Flash κ **(W m^{-1} K^{-1})**	**Optothermal Raman** κ **(W m^{-1} K^{-1})**	**Enhancement**	
PVDF-HFP-GN10	15.9 ± 0.3	16.4 ± 2.2	×81 times	7975%
PVDF-HFP-GN20	24.5 ± 0.3	26.6 ± 3.7	×128 times	12675%
PVDF-HFP-GN33	38.1 ± 0.2	37.7 ± 5.3	×190 times	18850%
PEMAA-GN10	15.2 ± 0.3	16.6 ± 2.3	×80 times	7850%
PEMAA-GN20	23.3 ± 0.5	22.2 ± 3.1	×114 times	11275%
PEMAA-GN33	41.8 ± 0.6	43.7 ± 6.1	×214 times	21275%

(a)

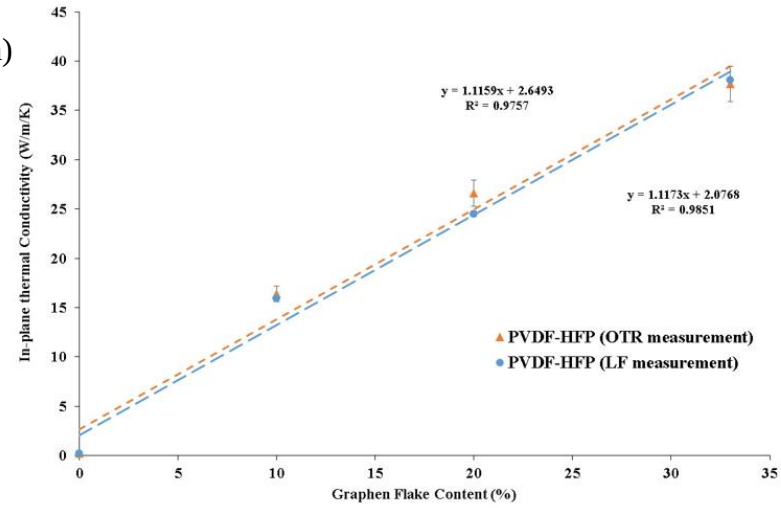

(b)

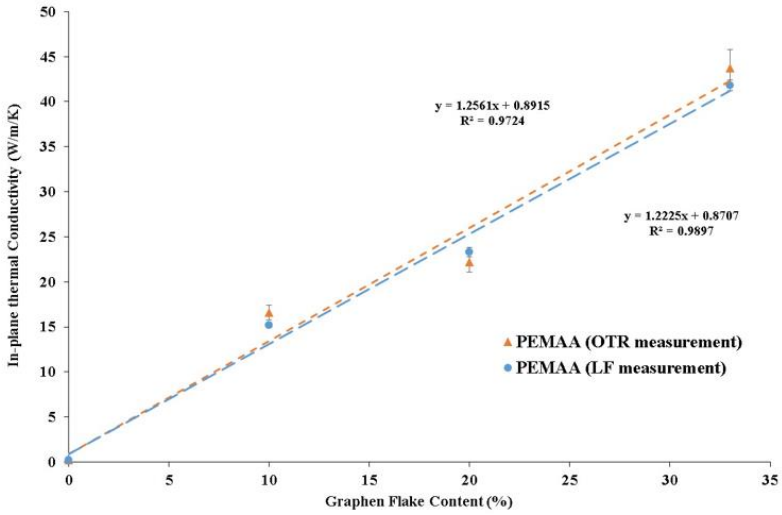

Figure 26 (a) In-plane thermal conductivity of graphene-based PVDF-HFP composites (b) In-plane thermal conductivity of graphene-based PEMAA composites

C. Studying the effect of Graphene average particle size on thermal, electrical, and mechanical properties of polymer composites obtained (Based on Paper 3)

The goal of this study was to understand the role of graphene particle size (average flake sizes of 7µm, 5µm, and 2µm) on the enhancement of electrical, thermal, and mechanical properties of poly(vinylidene fluoride-co-hexafluoropropylene) (PVDF-HFP) composites. The average particle size of each graphene type is 7 ± 0.35 µm, 5 ± 0.25 µm, and 2 ± 0.1 µm for G1, G2, G3, respectively. The average of three different lengths (L1, L2, and L3) was calculated for more than 50 samples, as shown in Figure 27. ATR-FTIR spectra of the three types of Graphene (G1, G2, and G3) are shown in Figure 28a. All three types had the same functional groups with two representative peaks for Graphene at 1547 cm^{-1} and 3651 cm^{-1} representing the skeletal vibrations of graphene backbone and –OH stretching vibrations respectively [68].

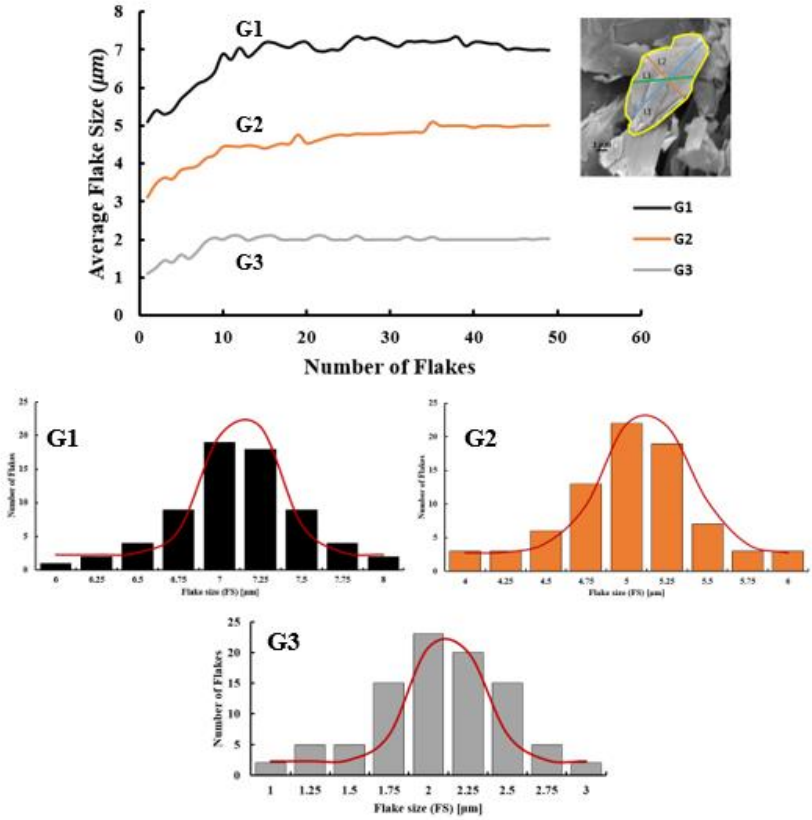

Figure 27 Statistical analysis of average flake size for the three different types of Graphene (G1, G2, and G3) as a function of the number of flakes taken into account. The average flake size converges to the asymptotic average values

Figure 28b shows the XRD patterns of the graphene flakes. A sharp peak at $2\theta=26.1^{\circ}$ corresponding to the crystalline structure of Graphene was observed noticeably for G1 and G2. This peak was relatively weak and broad for the G3 type indicating the low crystallinity of G3. The disappearance of this peak could mean that the distance between graphene sheets is irregular due to a high number of defects or that the number of graphene sheets per flake is very small. Raman spectra from the three types of Graphene are consistent with the former explanation. For G3, the intensity of the D peak was higher than the intensity of the G peak, which indicates the poor quality of G3 in comparison to G1 or G2, as shown in Figure 28e. The ratio of the intensity of D peak to G peak, which indicates the number of defects in Graphene is the highest

(I_D/I_G =1.08) for G3, which implies that more sp^3 defects are available in G3 than in G1 and G2 (I_D/I_G=0.74 and 0.83 respectively). Further, elemental analysis of the graphene flakes also showed that G3 had more impurities than G1 and G2, as the concentration of Nitrogen in G3 sample was noticeably higher than that in G1 and G2 (Figure 28f) [18].

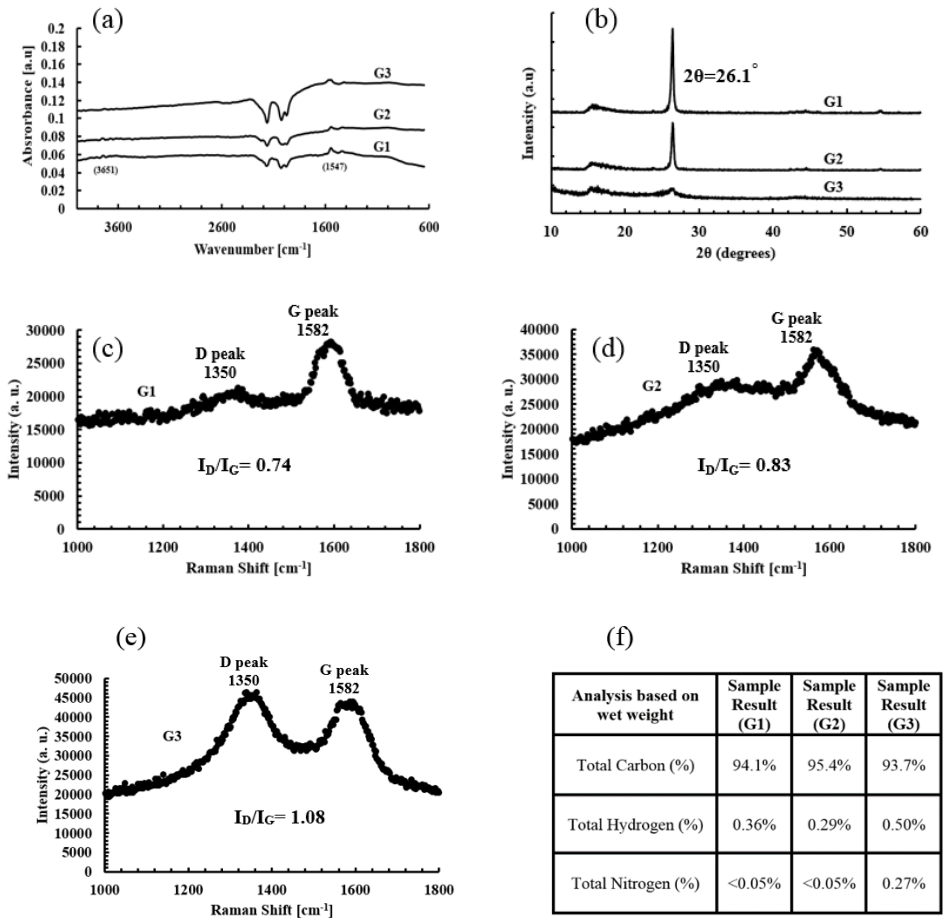

Analysis based on wet weight	Sample Result (G1)	Sample Result (G2)	Sample Result (G3)
Total Carbon (%)	94.1%	95.4%	93.7%
Total Hydrogen (%)	0.36%	0.29%	0.50%
Total Nitrogen (%)	<0.05%	<0.05%	0.27%

Figure 28 (a) ATR-FTIR analysis for G1, G2, and G3 (b) X-ray diffraction patterns for G1, G3, and G3 (c) Raman signal for G1 (d) Raman signal for G2 (e) Raman signal for G3 (f) Table showing the elemental analysis done on G1, G2, and G3

Graphene-based PVDF-HFP composites were fabricated using a solution-based method, as described in the previous section. The polymer composites showed very high values of electrical conductivity (Figure 29) and showed an enhanced electrical

conductivity in the order of flake size: G1>G2>G3. A record electrical conductivity of ~4445 S/m was measured for PVDF-HFP-G1-20. PVDF-HFP is an insulator with a very low electrical conductivity of 10^{-14} (S/m), and the aforementioned electrical conductivity corresponds to a significant improvement making these composites comparable to conductive metals such as stainless steel that has an electrical conductivity of ~ 2×10^{6} S/m [35].

Similar to metallic fillers in polymeric composites, the shape and size of graphene flakes have a significant influence on the electrical conductivity of obtained composites [69]. Lower conductivity is attributed to inferior quality and smaller size of G3 flakes. The former reduces the inherent conductivity of the flakes. At the same time, the latter means more inter-particle contacts are present in a conductive path resulting in a higher scattering rate of electrons at boundaries. G1 achieved the most significant increase in the electrical conductivity for graphene-based composites because large graphene flakes have larger density and smaller inter-sheet contact resistance. The electrical conductivity increased further after adding 5% and 10% of Graphene but with a slower rate due to typical percolation transition behavior for electrical conductivity in conductive polymeric composites [35,36]. SEM images showed that large planar flakes (G1 and G2) can be aligned in a plane much better than small round-shape (isotropic) graphene flakes (G3).

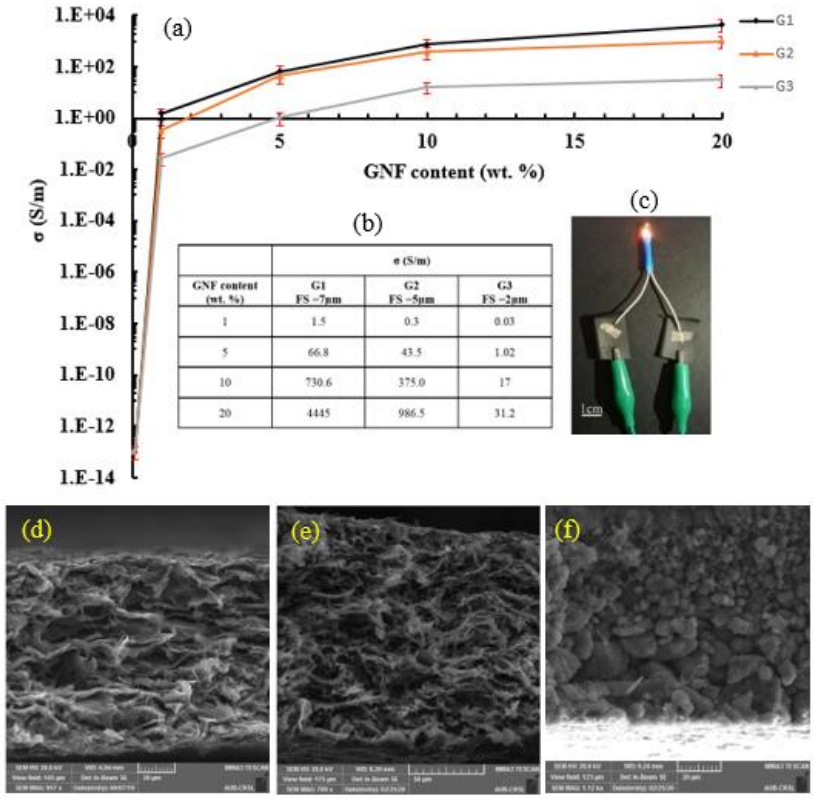

GNF content (wt. %)	σ (S/m) G1 FS ~7μm	G2 FS ~5μm	G3 FS ~2μm
1	1.5	0.3	0.03
5	66.8	43.5	1.02
10	730.6	375.0	17
20	4445	986.5	31.2

Figure 29 In-plane electrical conductivity as a function of graphene content (wt.%) for three different graphene types (a,b), and a picture showing a light bulb under 9V battery where PVDF-HFP-G1-20 film was used as an electrical connection (c). SEM micrographs

G1-based polymer composites showed the highest value for the in-plane thermal conductivity, which was also confirmed and reported before using a laser flash method [36,70]. An ultra-high value was achieved ~26 W/mK, which is one of the highest measured values for in-plane thermal conductivity for PVDF composites compared to the values reported in Table 2. For the same graphene wt%, the in-plane thermal conductivity value was lower for G2 and G3, respectively indicating that the average flake size also has a direct effect on the in-plane thermal conductivity values of the composites obtained. With larger graphene flakes, the density of filler/matrix interfaces is smaller, and the interfacial heat resistance (Kapitza resistance) will have less of an effect on the thermal conductivity [5]. G1 composites were more aligned and stacked in

an overlapping structure than G2 composites, as shown in Figures 30(d-e). Also, just as with electrical conductivity, the high defect concentration in G3 decreased the in-plane thermal conductivity of the flakes themselves obtained due to an increased rate of phonon-defect scattering mechanism [1].

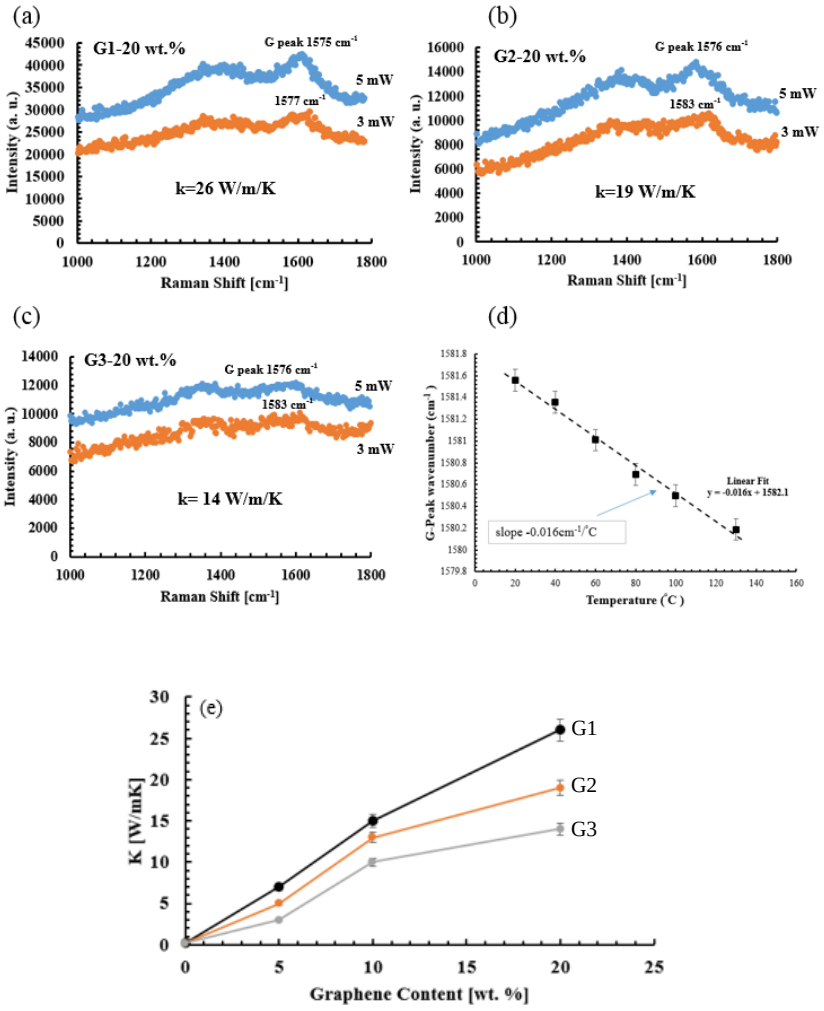

Figure 30 The Raman signals of Graphene-based composites (d) G-peak wavenumber versus Temperature (e) Enhancement of in-plane thermal conductivity as a function of Graphene content for three Graphene types G1, G2, and G3

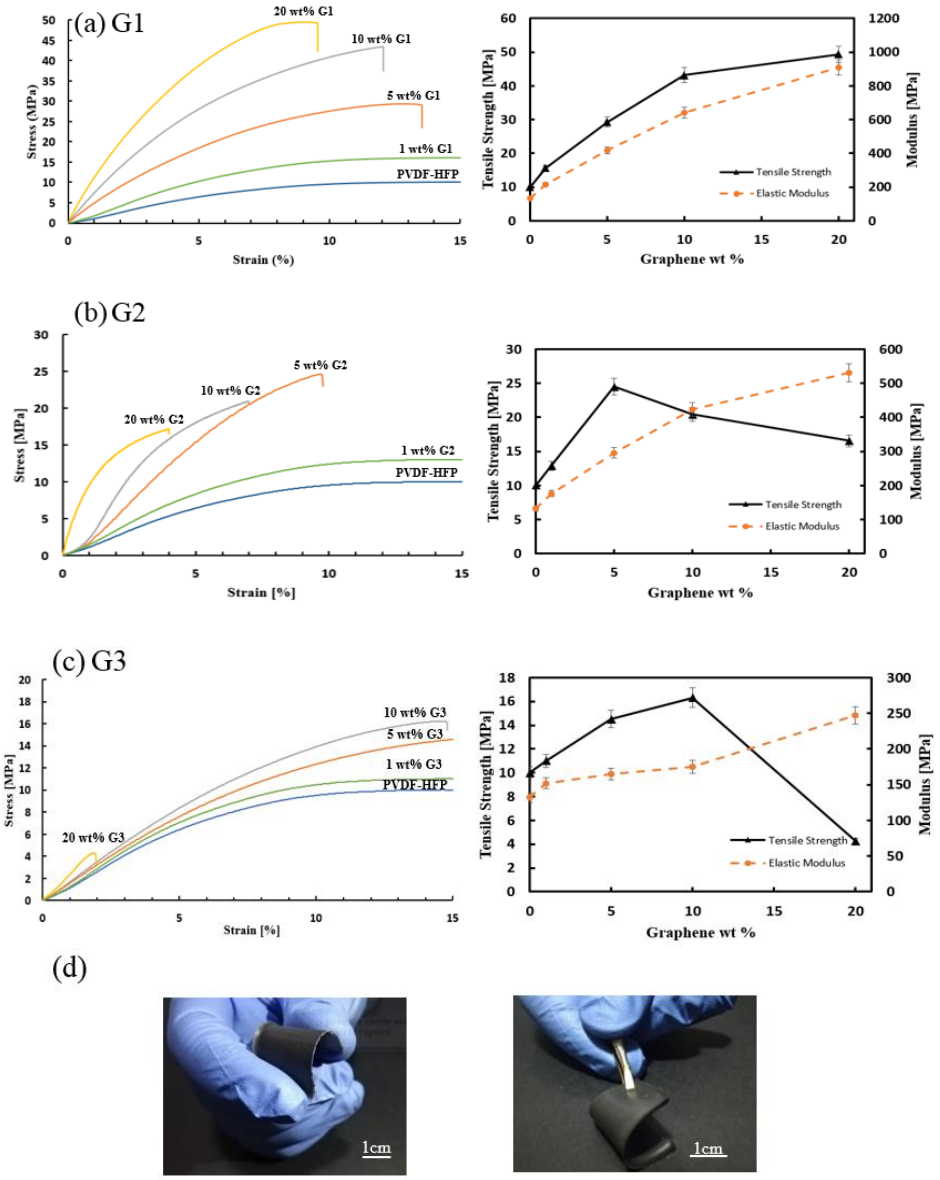

Figure 31 Mechanical properties as a function of Graphene content (wt %) for three different Graphene types (a) G1 (b) G2 (c) G3 (d) Two photos showing the flexibility of PVDF-HFP-G1-20. [colored figures]

Typical stress-strain curves for the composites are shown in Figure 31 with the values for the tensile strength and Young's modulus as a function of graphene content to the right. Figure 31a shows that increasing the concentration of the graphene flakes increases tensile strength; the tensile strength increased to ~ 50 MPa for 20 wt.% of G1. Also, the tensile strength for G1 composites was higher than the tensile strength for G2

and G3 composites with the same graphene loading. For example, for 5 wt % G1, the ultimate strength was ~26 MPa, whereas it was 24 MPa and 14.5 MPa for G2 and G3, respectively. These results showed that the size of the graphene flakes used is a significant factor that affects the tensile strength of the composites as large flakes tend to have a more compact and aligned structure for the composite than smaller flakes [59]. The significant enhancement in tensile strength is also due to its proper dispersion and adhesion with the matrix of PVDF-HFP [36]. The smaller response of small flakes may be due to a lower dispersion where chunks of Graphene (G3) can act as failure points in the composite.

D. The effect of temperature on thermal, electrical, and mechanical properties of polymer composites obtained (Based on Paper 4)

In this work, we studied the effect of temperature on the electrical, thermal, and mechanical properties of graphene-based poly(vinylidene fluoride-co-hexafluoropropylene) (PVDF-HFP) composites. Graphene-based polymer composites (PC-Gn) with various graphene content were prepared using solution mixing and molding process. Figure 32 shows the DSC thermograms of the PC-Gn films. A heating /cooling /heating process is very necessary to identify crystallization and melting peaks for semi-crystalline composite PC-Gn that may shift due to the difference in the composition of the polymer composites. For a neat PVDF-HFP copolymer the melting temperature is ~155 °C provided by the supplier. After adding 1 wt% of graphene and from the DSC diagrams in Figure 32a, PC-Gn 1% film exhibited an exothermic peak showing an average crystallization temperature (Tc) at 128.5 °C and an endothermic average peak (Tm) at 154.7 °C which is associated with the melting temperature of the

crystalline phase of the PVDF-HFP copolymer. This result agrees with the melting temperature value that was found by thermal gravimetric analysis (TGA) that was done by the authors in a previous publication [36]. The thermal stability of polymer composites is an important parameter that can be obtained from the TGA analysis. Previous analysis showed that the initial degradation temperature of the polymer composites was not affected by the addition of graphene filler up to 20 wt%. However, the carbon ash remaining of the polymer composites depended on the initial graphene content (%). With increasing graphene content (wt%), both peaks become broad for PC-Gn 10% and PC-Gn 20% as seen in Figure 32(b-c). This agrees with previous studies, where graphene flakes serve as an effective nucleating agent for PVDF-HFP composites and they encouraged the melt-crystallization rates of the composites for low graphene loading, but above certain levels, the fillers may hinder the movement of polymer chains, thus retarding the crystallization of the composite [43]. Also, the heat capacity of graphene change with temperature which may cause the change in the thermal capacity of the composite with Temperature as shown in Figure 32.

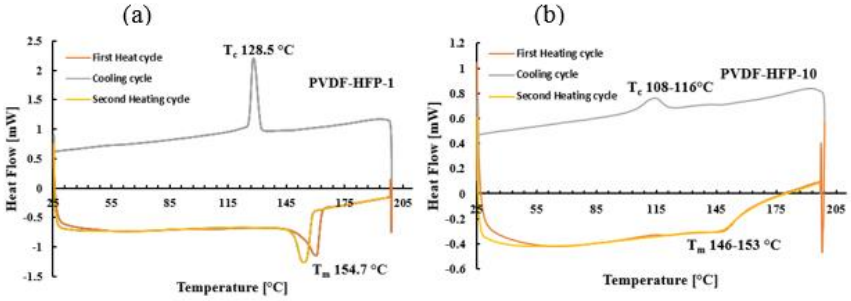

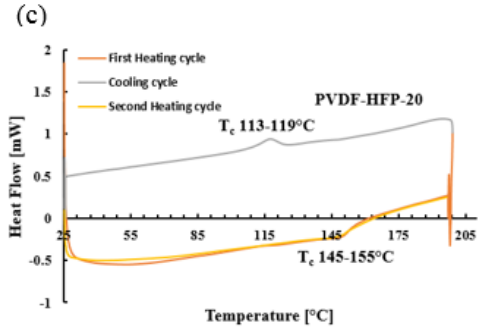

Figure 32 DSC diagrams of composite films: (a) PC-Gn 1% (b) PC-Gn 10% (c) PC-Gn 20 %

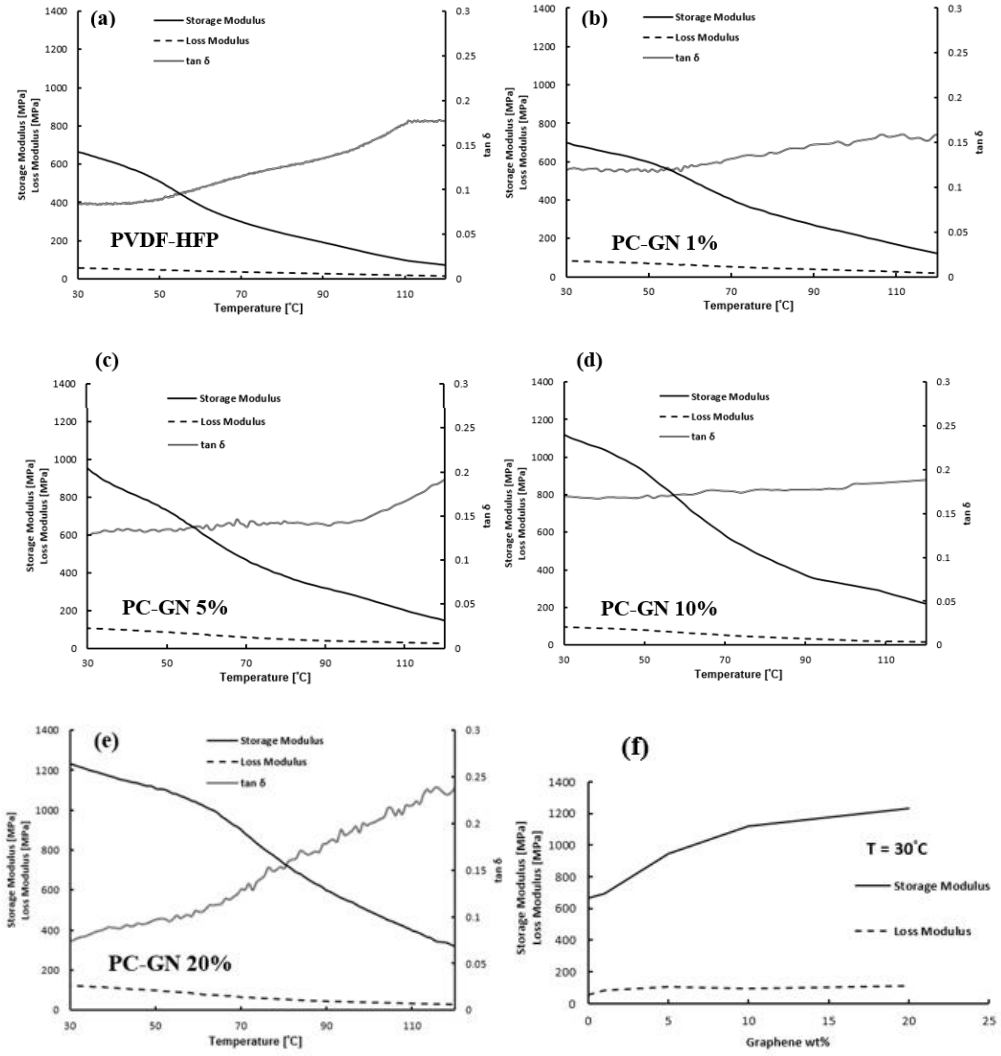

Figure 33 Storage modulus, loss modulus and tan δ curves from dynamic mechanical analysis (DMA) for the following films (a) PVDF-HFP (b) PC-Gn 1% (c) PC-Gn 5% (d) PC-Gn 10% (e) PC-Gn 20% (f) variation of storage modulus and loss modulus as a function of graphene

DMA is a common method used to study the viscoelastic mechanical properties of polymer composite materials. These mechanical properties are important to study the bonding between the filler and the matrix in any composite material. Using rectangular composite film samples, the storage modulus, loss modulus, and loss factor (tan δ) were measured across a temperature range between 30-120 °C as shown in Figure 33. The storage modulus sudden decrease indicates the transition between the glassy and the rubbery states of the polymer composite or the presence of molecular motion/rotation in the polymer composite. This is accompanied by having also a peak in the tan δ curve that is calculated as the ratio between the viscous and the elastic portion of the composite. Therefore, there was no sudden drop in the modulus for any of the composite films for the temperature range between 30-120 °C since the temperature range studied is beyond the glass transition temperature for the copolymer matrix PVDF-HPD which is ~ -35 °C. However, the presence of graphene flakes improves the stiffness of these composites since the storage modulus is higher with increasing graphene wt%. At the temperature of 30 °C, the storage modulus was 680 MPa for pure PVDF-HFP, the storage modulus increased to reach 1230 MPa with an increase of nearly 80% for PC-GN 20% as shown in Figure 33f. As graphene wt% increases in the composite, the mobility of the chains of PVDF-HFP copolymer is restricted due to the presence of these graphene flakes fillers making these composites more brittle [71]. Also, the loss modulus for all composites decreased with higher temperature as shown in Figure 33. As the temperature continues to increase above the glass transition temperature, the molecular frictions in the composites are reduced, thus less energy is dissipated which causes the loss modulus to decrease. Also, there were no peaks for the

loss factor (tan δ) curve which indicates that there is no major motion/rotation of the main chain backbone for the copolymer composite at the temperature range between 30-120 °C. Therefore, DMA results showed that there was no major molecular motion/rotation in the composites for the temperature range between 30-120 °C and there was a good integration between the filler (graphene flakes) and the polymer matrix (PVDF-HFP) which is compatible with the studies that the authors published before.

Figure 34 shows the electrical conductivity (EC) values of PC-Gn films as a function of temperature from 25 °C to 125 °C. Enhanced electrical conductivity was achieved with higher graphene wt% in the composites where graphene composites with 20 wt% achieved the highest electrical conductivity 4445 S/m at 25 °C and this electrical conductivity corresponds to a major improvement from the electrical conductivity for pure PVDF-HFP. PVDF-HFP, like other polymers, is an electrical insulator with a very low electrical conductivity which is around 10-14 (S/m), and this obtained electrical conductivity value of the composites corresponds to a huge enhancement of 17 orders of magnitude making these composites comparable to conductive metals 29. This improvement is attributed to many factors including (a) using pure conductive fillers of graphene flakes (i.e., graphene with 98.5% purity), (b) the dispersion of the graphene flakes across the polymer composites, (c) the good integration between the polymer matrix PVDF-HFP and graphene flakes as shown in DMA results in Figure 33, (d) graphene flakes were stacked on top of each other due to the slow gravitational settling of the graphene in PVDF-HFP matrix during the slow solvent evaporation process.

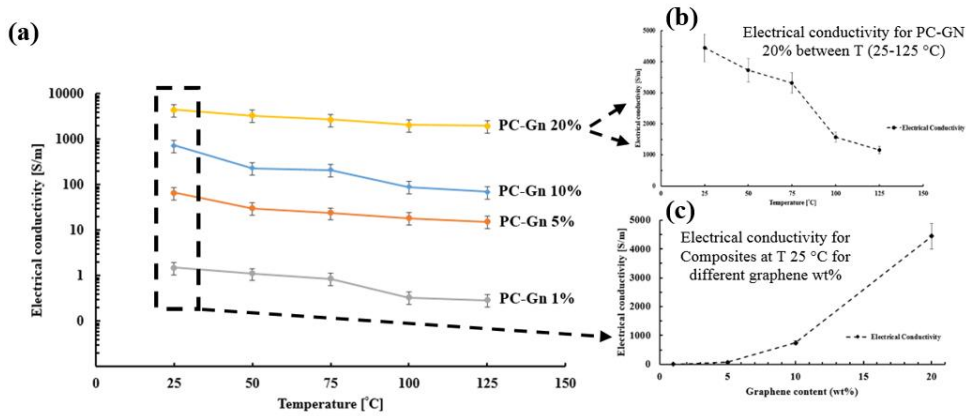

Figure 34(a) Electrical conductivity (EC) as a function of graphene content (wt%) across a temperature range between 25 °C and 125 °C for PC-Gn 1%, PC-Gn 5%, PC-Gn 10%, and PC-Gn 20% composite films (b) EC for PC-Gn 20% as a function of temperature (c) EC at T 25

The value of the electrical conductivity dramatically increased after adding 1 wt% of graphene flakes. The conductive graphene flakes form multiple conductive channels within these fabricated graphene-based PVDF-HFP composites, thus improving the conductivity of these composites with increasing graphene wt% based on a percolation model. Statistically, more conductive pathways can be generated by the addition of graphene flakes. Thus, the chance of overlapping between the flakes would be also higher with higher graphene wt % which can be estimated by a percolation model. As for the effect of temperature on the electrical conductivity of the composites obtained, both electrons and phonons exist in a carbon-based material. The trend of a decreasing conductivity is attributed to the fact that with increasing temperature, the probability of electron-phonon interaction increases rapidly, resulting in electrons being scattered by phonons at high temperatures which causes this decrease in the electrical conductivity at high temperatures for graphene-based PVDF-HFP composites. Similar to metals, the value of electrical conductivity of graphene-based polymer composites decreased with the increase of temperature. The lower conductivity is due to electron

scattering resulting in a sharp decrease in the mean free path of electrons. Graphene flakes were aligned in a plane creating conductive channels where electrons were able to pass across the polymer matrix that has a very low conductivity value. The energy of carbon atoms is at a low level when the temperature is low, however, they acquire more energy and start to vibrate across their mean positions when the temperature increases. Also graphene has a negative thermal expansion coefficient in the temperature range between 0 and 1000 K, so graphene flakes tend to contract as the temperature rises which can create more scattering and dispersion for the conductive path. Therefore, the electrical conductivity of the films is expected to decrease with temperature due to the collision activity of free electrons and carbon atoms in graphene. Moving electrons tend to collide easily with oscillating atoms thus reducing the conductivity of the composite films obtained for all graphene-based composites at high temperatures. This analysis agrees with previous studies that showed that high temperature affects the electrical properties of graphene and polymer, as well as on the characteristics of the interface between the graphene fillers and the polymer matrix [72,73].

There is extensive research ongoing to utilize graphene in batteries and supercapacitors for its superior electrical and electrochemical properties. There are many promising applications for graphene-based electrodes for both electrochemical double-layer capacitors and rechargeable lithium-ion batteries. Incorporating aligned graphene fillers into a flexible PVDF-HFP polymer matrix adds another dimension to the pool of application of this material. Thus, the electrochemical analysis was obtained for all PC-Gn films to study their performance as an electrode material, their electrochemical impedance under typical aqueous conditions, and their potential application in batteries. Figure 35a shows the cyclic voltammetry (CV) curves for all

the composite films of interest with CV curves for PVDF-HFP, PC-Gn 1%, PC-Gn 5% composites shown in the inset of the figure. Neat PVDF-HFP did not show any current density value across the voltage range between -0.4 V and 0.4V. As we added graphene to PVDF-HFP, the composites became conductive and the CV curves for PC-Gn 10 % and PC-Gn 20% show a typical rectangular behavior depicting an excellent super capacitive behavior. The CV curves become quasi parallelograms at the extreme voltages, which could be due to the intrinsic resistance of the stacked graphene flakes. The presented CV curves are in agreement with the previously reported CV curves of graphene electrodes. Figure 38b shows how the charge-storage capacity (CSC) (Area under the curve for the CV curve) increases significantly with increasing the percentage of graphene weight % in these composites. In comparison to commonly used materials that are used as electrodes as shown in Table 10, PC-Gn 20% composite has high charge storage comparable to Iridium oxide, Platinum, Tantalum/Ta_2O_5, and Titanium nitride which show the potential of these composites. These electro-chemical properties for graphene-based polymer composites allow researchers to use this material in next-generation batteries, super-capacitors, and bio-interfaces. Figure 35c shows the Electrochemical impedance (EIS) of all composite films. The impedance values dramatically decreased after adding just 1 wt% of graphene. The impedance continued to decrease for 5 wt%, 10 wt%, and 20 wt% of graphene but with a smaller factor, which could also be explained by the percolation transition behavior in conductive polymer composites. The decrease in the amplitude of the impedance spectrum following the addition of the graphene flakes can be related to the presence of conductive graphene channels on the surface of the composites which are confirmed in the SEM images complementing also the results of the electrical conductivity

measurements. Neat PVDF-HFP had a very high impedance in the range of 108 Ω but adding even 1% of graphene in the matrix would drop the value by nearly half as shown in Figure 35c. Additionally, the reduced impedance makes these graphene-based composites suitable for many applications in the future because it allows for a higher Signal-to-Noise Ratio (SNR) in any bio-potential recording.

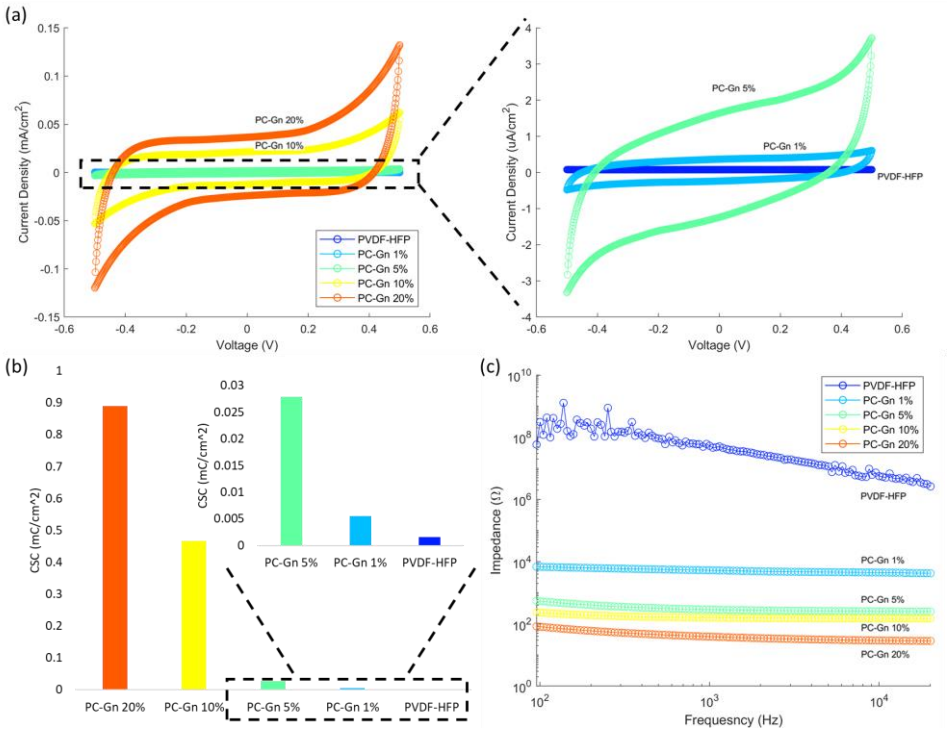

Figure 35 (a) CV, (b) CSC, (c) EIS for for PVDF-HFP, PC-Gn 1%, PC-Gn 5%, PC-Gn 10%, and PC-Gn 20% composite films

Table 6 Charge-storage capacity (CSC) for different materials used as electrodes

Electrode Material	CSC [mC/cm^2]	Reference
Iridium oxide	1-5	Shin et al.[74]
Platinum	0.05-0.15	Green et al.[75]
Tantalum/Ta_2O_5	0.5	Cogan et al.[76]
Titanium nitride	1	Cogan et al.[76]
PC-GN 20%	**0.9**	**This Study**

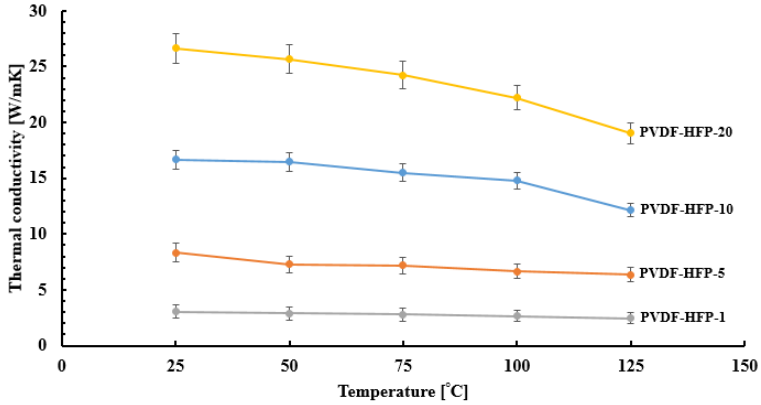

Figure 36 Thermal conductivity (TC) values for PC-Gn films as a function of temperature

Figure 36 represents the in-plane thermal conductivity values obtained for all the composite films at a temperature range between 25 °C to 125 °C using the Optothermal Raman method (OTR). The PC-Gn samples with higher graphene content had higher TC values. This can be attributed to the increase in thermal transport capacity (phonons movement) due to the proper alignment of graphene flakes in-plane across the composite films. Proper orientation of the graphene flakes within composite films would supply a direct path of lower thermal resistance for phonons to travel. The TC values gradually decreased by increasing the temperature for all the samples and this was more pronounced for the samples with higher graphene content. The highest value of in-plane TC (~26 W/mK) was obtained for PC-Gn 20% at 25 °C. This value decreased to 23 W/mK and 19 W/mK at temperatures 100 and 125 °C, respectively. Thermal conductivity in any material is governed by phonons and electrons movement, therefore the thermal conductivity value of the material is divided into two main parts: : $k = k_e + k_p$where k_e is the thermal conductivity due to electrons movement and k_p is thermal conductivity induced from atom interactions and collisions (phonons). Based on Wiedermann-Franz law, we can estimate the thermal conductivity due to movement of electrons:

$$k_e = L_0 \sigma_e T$$

where the thermal conductivity due to electrons (k_e) is the product of the Lorentz constant ($L_0 = 2.44 \times 10^{-8}\ W\Omega/\mathrm{K}^2$), electrical conductivity ((σ_e) and temperature (T). Thus, for our polymer composites, the highest value for in-plane electrical conductivity was 4445×10^3 S/m at a temperature of 25 °C, therefore the resulting electronic thermal conductivity would be eliminated since it is around 3×10^{-2} W/mK and it is less than 2% of the thermal conductivity of the material. Therefore, phonons are the main carriers of heat for these composites. However, phonons can be scattered through several mechanisms including phonon-impurity scattering, Umklapp phonon-phonon scattering which happens mainly in crystalline materials, phonon-electron scattering, and phonon-boundary scattering. The graphene we used was 98.8% pure and the thermal measurements were performed at room temperature and above so that the rate of phonon-impurity scattering was minimized because in the measured temperature range phonon-impurity scattering is unlikely. With increasing temperature, the phonon-phonon scattering rate is expected to increase which may be the reason behind this decrease in the thermal conductivity values of these composites as shown in Figure 36. As thermal conductivity is related to establishing a thermal pathway in the polymeric matrix that allows phonons to transport more efficiently and reducing phonon scattering mechanisms. This analysis is compatible with previous studies that attributed the observed dependence of thermal conductivity on temperature to the severe vibration of composite fillers at high temperatures, which strongly impeded the movement of both electrons and phonons across the composite films decreasing the in-plane thermal conductivity values. Also, graphene weight % affects the temperature dependence of thermal conductivity of obtained polymer composites. For a low weight of graphene,

the thermal conductivity of the composite film is weakly temperature-dependent, indicating that the scattering of phonons by mass fluctuation and boundaries are the dominant phonon scattering mechanisms in the measured film (as these scattering processes are temperature-independent). However, as the weight of graphene increases, the temperature dependence of thermal conductivity increases, indicating a predominance of phonon-phonon scattering processes, which are temperature-dependent. However, the in-plane thermal conductivity for PC-Gn 20% at T 125 °C remains higher than the thermal conductivity of PC-Gn 10% at T 25 ^{0}C, which shows that more conductive channels were established with higher graphene content (wt%) allowing these composites to have higher in-plane thermal and electrical conductivities as shown in Figures 34 and 36.

CHAPTER V
SUMMARY AND CONCLUSIONS

Graphene-based polymer composites were successfully fabricated, tested and proved to have ultra-high thermal and electrical conductivity values. These conductive composites can be an auspicious material that can used in many new applications in many industries. Promising results in the properties of the obtained composites were achieved, which shows the importance of this project. Adding Graphene flakes in a polymer matrix has been employed before for physical and mechanical enhancement. However, the properties for produced composites did not reach the expected values estimated by the rule of mixing due to many parameters involved like (type of Graphene used, preparation process, morphology, number of layers, the orientation of Graphene in the polymer matrix, the loading of Graphene, and the interface between Graphene and the polymer matrix). In this thesis, we discovered an innovative preparation process with optimized parameters to fabricate conductive polymers. The integration of Graphene flakes with two polymer matrices (PVDF and PEMAA) was studied as we characterized the morphology of obtained films using different techniques (SEM, ATR-FTIR, and Optical tensiometer). Moreover, we prepared composite films with three different types of Graphene with various average flake size (G1, G2, and G3). We analyzed the thermal, electrical, and mechanical properties of obtained composites using adequate techniques (laser-flash analysis, OTR, stress-strain, and electrical conductivity analysis). This shed light on the effect of Graphene average flake size on the properties of the obtained composite films. Composites with Graphene flakes that have large average particle size show high thermal and electrical conductivity values

also high mechanical properties to a certain extent. In addition to that, we studied the effect of temperature on the thermal, electrical, and mechanical properties of obtained composites. The in-plane electrical and thermal conductivity values of the graphene based composites decreased linearly by increasing temperature. However, the polymer composites remained conductive even at a temperature as high as 125 °C. For a low weight of graphene, the conductivity of the composite film is weakly temperature dependent, indicating a high rate of scattering of phonons by mass fluctuation and boundaries. However, as the content of graphene increases in the film, the temperature dependence of thermal conductivity increases, indicating a predominance of phonon–phonon scattering processes, which are temperature-dependent. Also, obtained graphene-based composites films showed promising electrochemical performance in a wide temperature range. Consequently, these composites can be used in several applications such as smart textiles, wearable sensors, and batteries in the future. Future Plans for this study include: (1) Trying new preparation processes like air brush and coating techniques (2) Testing graphene in textile and use it in sensing applications (3) Working on a proper simulation model that can help in measuring thermal and electrical conductivity values for graphene-based composites.

APPENDIX A

LIST OF PUBLICATIONS

The results that were obtained in this thesis were published in top tier international journals. These publications have been cited by many researchers around the world. Also, some of the results have been presented in international conferences in Spain, Hungary, and Lebanon. Below are some of the papers that were published based on the following project:

1. **A.A. Tarhini**, A.R. Tehrani-Bagha, Graphene-based polymer composite films with enhanced mechanical properties and ultra-high in-plane thermal conductivity, Compos. Sci. Technol. (2019) 107797. doi:10.1016/J.COMPSCITECH.2019.107797 **(Paper 1)**

2. **A. Tarhini**, A.R. Tehrani-Bagha, M. Kazan, Graphene-based polymer composites with ultra-high in-plane thermal conductivity: A comparison study between optothermal Raman spectroscopy and laser flash method, J. Appl. Polym. Sci. 48927 (2020) 1–8. doi:10.1002/app.48927 **(Paper 2)**

3. **A Tarhini**, A Tehrani-Bagha, M Kazan, B Grady, "The effect of graphene flake size on the properties of graphene-based polymer composite films", Journal of Applied Polymer Science, 49821 **(Paper 3)**

4. **A. Tarhini**, M.W. Alchamaa, M. Khraiche, M. Kazan, A. Tehrani-Bagha, The effect of temperature on the electrical and thermal conductivity of graphene-based polymer composite films, J. Appl. Polym. Sci. (2021) 51896. doi:10.1002/app.51896. **(Paper 4)**

5. A Aryanfar, S Medlej, **A Tarhini**, A Tehrani, “Elliptic Percolation Model for Predicting the Electrical Conductivity of Graphene-Polymer Composites”, Soft Matter **(Paper 5)**
6. A. Aryanfar, S. Medlej, **A. Tarhini**, S.R. Damadi, A.R. Tehrani B., W.A. Goddard, 3D percolation modeling for predicting the thermal conductivity of graphene-polymer composites, Comput. Mater. Sci. 197 (2021) 110650. doi:10.1016/j.commatsci.2021.110650. **(Paper 6)**

REFERENCES

[1] A. Henry, THERMAL TRANSPORT IN POLYMERS, Annu. Rev. Heat Transf. 17 (2014) 485–520. doi:10.1615/AnnualRevHeatTransfer.2013006949.

[2] Y. Huang, S. Kormakov, X. He, X. Gao, X. Zheng, Y. Liu, Conductive Polymer Composites from Renewable Resources : An Overview of Preparation , Properties , and Applications, Polymers (Basel). (2019) 1–32. doi:10.3390/polym11020187.

[3] X. Huang, P. Jiang, T. Tanaka, A Review of Dielectric Polymer Composites With High Thermal Conductivity, IEEE Electr. Insul. Mag. 27 (2011) 8–16. doi:10.1109/MEI.2011.5954064.

[4] Z. Han, A. Fina, Thermal conductivity of carbon nanotubes and their polymer nanocomposites: A review, Prog. Polym. Sci. 36 (2011) 914–944. doi:10.1016/j.progpolymsci.2010.11.004.

[5] N. Burger, A. Laachachi, M. Ferriol, M. Lutz, V. Toniazzo, D. Ruch, Review of thermal conductivity in composites: Mechanisms, parameters and theory, Prog. Polym. Sci. 61 (2016) 1–28. doi:10.1016/j.progpolymsci.2016.05.001.

[6] L. Liu, X. Bian, J. Tang, H. Xu, Z. Hou, W. Song, RSC Advances properties in tunable all-graphene papers, R. Soc. Chem. 5 (2015) 75239–75247. doi:10.1039/c5ra15533a.

[7] B.Y. Zhu, S. Murali, W. Cai, X. Li, J.W. Suk, J.R. Potts, R.S. Ruoff, Graphene and Graphene Oxide: Synthesis, Properties, and Applications, Adv. Mater. 22 (2010) 3906–3924. doi:10.1002/adma.201001068.

[8] D. Li, M.B. Muller, S. Gilje, E. Al, Processable aqueous dispersions of graphene nanosheets, (2008) 101–105. doi:10.1038/nnano.2007.451.

[9] V.H. Boehh, A. Clauss, G. Fischer, U. HOFMANN, Das Adsorptionsverhalten - sehr dunner Ko hlenstoff Folien Voii, J. Inorg. Gen. Chem. 316 (1962) 119–127. doi:10.1002/zaac.19623160303.

[10] A.A. Balandin, S. Ghosh, W. Bao, I. Calizo, D. Teweldebrhan, F. Miao, C.N. Lau, Superior Thermal Conductivity of Single-Layer Graphene, Nano Lett. 8 (2008) 902–907. doi:10.1021/nl0731872.

[11] S. Ghosh, I. Calizo, D. Teweldebrhan, E. Al, Extremely high thermal conductivity of graphene: Prospects for thermal management applications in nanoelectronic circuits, Appl. Phys. Lett. 92 (2008) 1–4. doi:10.1063/1.2907977.

[12] A.A. Balandin, In-plane and cross-plane thermal conductivity of graphene: Applications in thermal interface materials, in: Carbon Nanotub. Graphene, Assoc. Devices IV, 2011. doi:10.1117/12.894455.

[13] C. Lee, X. Wei, J.W. Kysar, J. Hone, Measurement of the Elastic Properties and Intrinsic Strength of Monolayer Graphene, Science (80-.). 321 (2008) 385–388. doi:10.1126/science.1157996.

[14] H.S. Dong, S.J. Qi, Realising the potential of graphene-based materials for biosurfaces – A future perspective, in: Biosurface and Biotribology, 2015: pp. 229–248. doi:10.1016/j.bsbt.2015.10.004.

[15] T. Tite, C. Donnet, A.S. Loir, S. Reynaud, J.Y. Michalon, F. Vocanson, F. Garrelie, Graphene-based textured surface by pulsed laser deposition as a robust platform for surface enhanced Raman scattering applications, Appl. Phys. Lett. 104 (2014) 3–7. doi:10.1063/1.4863824.

[16] V. Singh, D. Joung, L. Zhai, S. Das, Graphene based materials: Past, present and future, Prog. Mater. Sci. 56 (2011) 1178–1271. doi:10.1016/j.pmatsci.2011.03.003.
[17] M. Cao, C. Du, H. Guo, X. Li, S. Song, Paving thermally conductive highway by 3D interconnected framework of carbon nanotube and graphene oxide in poly(vinylidene fluoride), Compos. Part A. 115 (2018) 331–340. doi:10.1016/j.compositesa.2018.09.024.
[18] H. Kim, A.A. Abdala, C.W. Macosko, Graphene/Polymer Nanocomposites, Macromolecules. 43 (2010) 6515–6530. doi:10.1021/ma100572e.
[19] J.& D.G.R. William D. Callister, Materials Science and Engineering An Introduction (8th edition), 1997.
[20] C.L. Choy, Thermal conductivity of polymers, Polymer (Guildf). 18 (1977) 984–1004. doi:https://doi.org/10.1016/0032-3861(77)90002-7.
[21] Y. Cao, M. Liang, Z. Liu, Enhanced thermal conductivity for poly(vinylidene fluoride) composites with nano-carbon fillers, R. Soc. Chem. 6 (2016) 68357–68362. doi:10.1039/c6ra11178e.
[22] H. Jung, S. Yu, N.S. Bae, S.M. Cho, R.H. Kim, S.H. Cho, I. Hwang, B. Jeong, J.S. Ryu, J. Hwang, S.M. Hong, C.M. Koo, C. Park, High Through-Plane Thermal Conduction of Graphene Nanoflake Filled Polymer Composites Melt-Processed in an L-Shape Kinked Tube, ACS Appl. Mater. Interfaces. 7 (2015) 15256–15262. doi:10.1021/acsami.5b02681.
[23] P. Xu, J. Loomis, R.D. Bradshaw, B. Panchapakesan, Load transfer and mechanical properties of chemically reduced graphene reinforcements in polymer composites, Nanotechnology. 23 (2012). doi:10.1088/0957-4484/23/50/505713.
[24] M.L. Clingerman, J.A. King, K.H. Schulz, J.D. Meyers, Evaluation of Electrical Conductivity Models for Conductive Polymer Composites, J. Appl. Polym. Sci. 83 (2002) 1341–1356. doi:10.1002/app.10014.
[25] A.J. Marsden, D.G. Papageorgiou, C. Vallés, A. Liscio, V. Palermo, M.A. Bissett, R.J. Young, I.A. Kinloch, Electrical percolation in graphene–polymer composites, 2D Mater. 6 (2018).
[26] D.G. Papageorgiou, I.A. Kinloch, R.J. Young, Mechanical properties of graphene and graphene-based nanocomposites, Prog. Mater. Sci. 90 (2017) 75–127. doi:10.1016/j.pmatsci.2017.07.004.
[27] G. Eda, Y.-Y. Lin, S. Miller, Transparent and conducting electrodes for organic electronics from reduced graphene oxide, 233305 (2009) 10–13. doi:10.1063/1.2937846.
[28] I. Ahmad, J. McCarthy, A. Baranov, Y. Gun'ko, Development of Graphene Nano-Platelet Based Counter Electrodes for Solar Cells, Materials (Basel). 8 (2015) 5953–5973. doi:10.3390/ma8095284.
[29] Z. Song, T. Xu, M.L. Gordin, Y.-B. Jiang, I.-T. Bae, Q. Xiao, H. Zhan, J. Liu, D. Wang, Polymer–Graphene Nanocomposites as Ultrafast-Charge and -Discharge Cathodes for Rechargeable Lithium Batteries, Nano Lett. 12 (2012) 2205–2211. doi:10.1021/nl2039666.
[30] Q. Wu, Y. Xu, Z. Yao, A. Liu, G. Shi, Supercapacitors Based on Flexible Graphene/Polyaniline Nanofiber Composite Films, ACS Nano. 4 (2010) 1963–1970.
[31] L. Lv, W. Dai, A. Li, L. Cheng-Te, Graphene-Based Thermal Interface Materials: An Application-Oriented Perspective on Architecture Design, Polymers (Basel).

10 (2018) 1201. doi:10.3390/polym10111201.
[32] S. Sayyar, E. Murray, B.C. Thompson, J. Chung, D.L. O, S. Gambhir, Processable conducting graphene/chitosan hydrogels for tissue engineering, J. Mater. Chem. B. (2015) 481–490. doi:10.1039/c4tb01636j.
[33] J.P. Bahamonde, H.N. Nguyen, S.K. Fanourakis, D.F. Rodrigues, Recent advances in graphene - based biosensor technology with applications in life sciences, J. Nanobiotechnology. (2018) 1–17. doi:10.1186/s12951-018-0400-z.
[34] G. Kaur, R. Adhikari, P. Cass, M. Bown, P. Gunatillake, Electrically conductive polymers and composites for biomedical applications, R. Soc. Chem. (2015) 37553–37567. doi:10.1039/c5ra01851j.
[35] P. Kumar, S. Yu, F. Shahzad, S.M. Hong, Y.H. Kim, C.M. Koo, Ultrahigh electrically and thermally conductive self-aligned graphene/polymer composites using large-area reduced graphene oxides, Carbon N. Y. 101 (2016) 120–128. doi:10.1016/j.carbon.2016.01.088.
[36] A.A. Tarhini, A.R. Tehrani-Bagha, Graphene-based polymer composite films with enhanced mechanical properties and ultra-high in-plane thermal conductivity, Compos. Sci. Technol. 184 (2019) 107797. doi:10.1016/j.compscitech.2019.107797.
[37] R. Qian, J. YU, C. Wu, Alumina-coated graphene sheet hybrids for electrically insulating polymer composites with high thermal conductivity, R. Soc. Chem. 3 (2013) 17373–17379. doi:10.1039/c3ra42104j.
[38] J. Yu, R. Qian, P. Jiang, Enhanced Thermal Conductivity for PVDF Composites with a Hybrid Functionalized Graphene Sheet-Nanodiamond Filler, Fibers Polym. 14 (2013) 1317–1323. doi:10.1007/s12221-013-1317-7.
[39] F.E. Alam, W. Dai, M. Yang, S. Du, X. Li, J. Yu, In situ formation of a cellular graphene framework thermal conductivity, R. Soc. Chem. 5 (2017) 6164–6169. doi:10.1039/c7ta00750g.
[40] Y. Chen, J. Gao, Q. Yan, X. Hou, S. Shu, M. Wu, N. Jiang, X. Li, J. Xu, C. Lin, J. Yu, Advances in graphene-based polymer composites with high thermal conductivity, VERUSCRIPT Funct. Nanomater. (2018). doi:https://doi.org/10.22261/OOSB06.
[41] J. Yu, X. Huang, C. Wu, P. Jiang, Permittivity , Thermal Conductivity and Thermal Stability of Poly (vinylidene fluoride)/ Graphene Nanocomposites, IEEE Trans. Dielectr. Electr. Insul. 18 (2011) 478–484. doi:10.1109/TDEI.2011.5739452.
[42] X. Zhao, Q. Zhang, D. Chen, P. Lu, Enhanced Mechanical Properties of Graphene-Based Poly(vinyl alcohol) Composites, Macromolecules. 43 (2010) 2357–2363. doi:10.1021/ma902862u.
[43] H.C. Bidsorkhi, A.G. D'Aloia, G. De Bellis, A. Proietti, A. Rinaldi, M. Fortunato, P. Ballirano, M.P. Bracciale, M.L. Santarelli, M.S. Sarto, Nucleation effect of unmodified graphene nanoplatelets on PVDF/GNP film composites, Mater. Today Commun. 11 (2017) 163–173. doi:10.1016/j.mtcomm.2017.04.001.
[44] J.C.M. Garnett, Colours in Metal Glasses , in Metallic Films , and in Metallic Solutions, Philos. Trans. R. Soc. London. 205 (1906) 237–288. doi:https://www.jstor.org/stable/90933.
[45] R.C. Progelhof, Methods for Predicting the Thermal Conductivity of Composite Systems : A Review, Polym. Eng. Sci. 76 (1976).

doi:https://doi.org/10.1002/pen.760160905.
[46] W.E.I. Lin, R. Zhang, C.P. Wong, Modeling of Thermal Conductivity of Graphite Nanosheet Composites, Electron. Mater. 39 (2010) 268–272. doi:10.1007/s11664-009-1062-2.
[47] S.N. Tripathi, G.S.S. Rao, A.B. Mathur, R. Jasra, Polyolefin/graphene nanocomposites: a review, R. Soc. Chem. (2017) 23615–23632. doi:10.1039/c6ra28392f.
[48] H.H. Horowitz, G. Metzger, A New Analysis of Thermogravimetric Traces, Anal. Chem. 35 (1963) 1464–1468. doi:10.1021/ac60203a013.
[49] C.W. Shao, Y.L. Liu, Y.C. Chiu, Y.S. Chiu, Thermal stability of epoxy resins containing flame retardant components: an evaluation with thermogravimetric analysis, Polym. Degredation Stab. 78 (2002) 41–48. doi:https://doi.org/10.1016/S0141-3910(02)00117-9.
[50] D.R. Askeland, P.P. Fulay, W.J. Wright, The Science And Engineering of Materials - 6th Edition, 2010. doi:10.1007/978-1-4899-2895-5.
[51] J. Chen, H. Lu, J. Yang, Y. Wang, X. Zheng, C. Zhang, Effect of organoclay on morphology and electrical conductivity of PC/PVDF/CNT blend composites, Compos. Sci. Technol. 94 (2014) 30–38. doi:10.1016/j.compscitech.2014.01.010.
[52] L.N. Sim, S.R. Majid, A.K. Arof, FTIR studies of PEMA/PVdF-HFP blend polymer electrolyte system incorporated with LiCF3SO3 salt, Vib. Spectrosc. 58 (2012) 57–66. doi:10.1016/j.vibspec.2011.11.005.
[53] S. Lee, Crystal Structure and Thermal Properties of Poly (vinylidene fluoride-hexafluoropropylene) Films Prepared by Various Processing Conditions, Fibers Polym. 12 (2011) 1030–1036. doi:10.1007/s12221-011-1030-3.
[54] Z. He, Q. Cao, B. Jing, X. Wang, Y. Deng, Gel electrolytes based on poly(vinylidenefluoride- co-hexafluoropropylene)/thermoplastic polyurethane/poly(methyl methacrylate) with in situ SiO2 for polymer lithium batteries, R. Soc. Chem. 7 (2017) 3240–3248. doi:10.1039/c6ra25062a.
[55] H. Kim, C. Mattevi, M.R. Calvo, Activation Energy Paths for Graphene Nucleation and Growth on Cu, ASC Nano. 6 (2012) 3614–3623. doi:10.1021/nn3008965.
[56] Q. Lv, D. Wu, Y. Qiu, J. Chen, X. Yao, K. Ding, Crystallization of Poly(e-caprolactone) composites with graphite nanoplatelets: Relations between nucleation and platelet thickness Qiaolian, Thermochim. Acta. 612 (2015) 25–33. doi:10.1016/j.tca.2015.05.005.
[57] S. Vadukumpully, J. Paul, N. Mahanta, S. Valiyaveettil, Flexible conductive graphene/poly(vinyl chloride) composite thin films with high mechanical strength and thermal stability, Carbon N. Y. 49 (2010) 198–205. doi:10.1016/j.carbon.2010.09.004.
[58] H. Wu, L.T. Drzal, Graphene nanoplatelet paper as a light-weight composite with excellent electrical and thermal conductivity and good gas barrier properties, Carbon N. Y. 50 (2012) 1135–1145. doi:10.1016/j.carbon.2011.10.026.
[59] P. Kumar, F. Shahzad, S. Yu, S.M. Hong, Y.H. Kim, C.M. Koo, Large-area reduced graphene oxide thin film with excellent thermal conductivity and electromagnetic interference shielding effectiveness, Carbon N. Y. 94 (2015) 494–500. doi:10.1016/j.carbon.2015.07.032.
[60] A. Li, C. Zhang, Y.-F. Zhang, Thermal Conductivity of Graphene-Polymer Composites: Mechanisms, Properties, and Applications, Polymers (Basel). 9

(2017) 437. doi:10.3390/polym9090437.
[61] S.J. Kalista, T.C. Ward, Z. Oyetunji, Self-healing of poly(ethylene-co-methacrylic acid) copolymers following projectile puncture, Mech. Adv. Mater. Struct. 14 (2007) 391–397. doi:10.1080/15376490701298819.
[62] V.T. Srikar, A.K. Swan, M.S. Ünlü, B.B. Goldberg, S.M. Spearing, Micro-Raman measurements of bending stresses in Micromachined Silicon Flexures, J. Microelectromechanical Syst. 12 (2003) 779–787. doi:10.1109/JMEMS.2003.820280.
[63] M. Nonnenmacher, H.K. Wickramasinghe, Scanning probe microscopy of thermal conductivity and subsurface properties, Appl. Phys. Lett. 168 (2000). doi:https://doi.org/10.1063/1.108207.
[64] P. Fan, L. Wang, J. Yang, F. Chen, M. Zhong, Graphene/poly(vinylidene fluoride) composites with high dielectric constant and low percolation threshold, Nanotechnology. 23 (2012).
[65] L. He, S.C. Tjong, A graphene oxide–polyvinylidene fluoride mixture as a precursor for fabricating thermally reduced graphene oxide–polyvinylidene fluoride composites, RSC Adv. (2013) 22981–22987. doi:10.1039/c3ra45046e.
[66] Y.C. Li, S.C. Tjong, R.K.Y. Li, Electrical conductivity and dielectric response of poly (vinylidene fluoride)– graphite nanoplatelet composites, Synth. Met. 160 (2010) 1912–1919. doi:10.1016/j.synthmet.2010.07.009.
[67] K.B. and S.R. Varrla Eswaraiah, One-pot synthesis of conducting graphene–polymer composites and their strain sensing application, Nanoscale. (2012) 1258–1262. doi:10.1039/c2nr11555g.
[68] B. Kartick, S.K. Srivastava, I. Srivastava, Green Synthesis of Graphene, J. Nanosci. Nanotechnol. (2013).
[69] Q. Xue, The influence of particle shape and size on electric conductivity of metal–polymer composites, Eur. Polym. J. 40 (2004) 323–327. doi:10.1016/j.eurpolymj.2003.10.011.
[70] A. Tarhini, A.R. Tehrani-Bagha, M. Kazan, Graphene-based polymer composites with ultra-high in-plane thermal conductivity: A comparison study between optothermal Raman spectroscopy and laser flash method, J. Appl. Polym. Sci. 137 (2020) 48927. doi:10.1002/app.48927.
[71] A. Tarhini, A. Tehrani-Bagha, M. Kazan, B. Grady, The effect of graphene flake size on the properties of graphene-based polymer composite films, J. Appl. Polym. Sci. 138 (2021) 49821. doi:10.1002/app.49821.
[72] X. Xia, G.J. Weng, J. Zhang, Y. Li, The effect of temperature and graphene concentration on the electrical conductivity and dielectric permittivity of graphene–polymer nanocomposites, Acta Mech. 231 (2020) 1305–1320. doi:10.1007/s00707-019-02588-4.
[73] A. Király, F. Ronkay, Temperature dependence of electrical properties in conductive polymer composites, Polym. Test. 43 (2015) 154–162. doi:10.1016/j.polymertesting.2015.03.011.
[74] S. Shin, J. Kim, J. Jeong, T.M. Gwon, G.J. Choi, S.E. Lee, J. Kim, S.B. Jun, J.W. Chang, S.J. Kim, High charge storage capacity electrodeposited iridium oxide film on liquid crystal polymer-based neural electrodes, Sensors Mater. 28 (2016) 243–260. doi:10.18494/SAM.2016.1175.
[75] R.A. Green, K.S. Lim, W.C. Henderson, R.T. Hassarati, P.J. Martens, N.H. Lovell, L.A. Poole-Warren, Living electrodes: Tissue engineering the neural

interface, Proc. Annu. Int. Conf. IEEE Eng. Med. Biol. Soc. EMBS. (2013) 6957–6960. doi:10.1109/EMBC.2013.6611158.
[76] S.F. Cogan, Neural Stimulation and Recording Electrodes, Annu. Rev. Biomed. Eng. 10 (2008) 275–309. doi:10.1146/annurev.bioeng.10.061807.160518.